Hindawi
Dermatologic Therapy
Volume 2023, Article ID 7950026, 21 pages
https://doi.org/10.1155/2023/7950026

Research Article

Role of Royal Jelly Treated Adipose-Derived Stem Cell-Extracellular Vesicles on Fibroblast Proliferation, Migration, and Collagen Production

Tomohiro Itoh,[1] **Tomomi Degawa**,[2,3] **Yuko Ito**,[4] **Yukihiro Akao**,[5] **and Nobuaki Okumura**[2,3]

[1]*Laboratory for Molecular Chemistry of Aquatic Materials, Department of Life Sciences, Graduate School of Bioresources, Mie University, 1577 Kurimamachiya, Tsu, Mie 514-8507, Japan*
[2]*Institute for Bee Products and Health Science, Yamada Bee Company Inc., Tomatagun, Okayama 708-0393, Japan*
[3]*Group Cosmetic Central Laboratory, Yamada Bee Company Inc., Shinagawa, Tokyo 104-0004, Japan*
[4]*Department of General and Gastroenterological Surgery, Osaka Medical Pharmaceutical College, 2-7 Daigaku-machi, Takatsuki, Osaka 569-8686, Japan*
[5]*United Graduate School of Drug Discovery and Medical Information Sciences, Gifu University, 1-1 Yanagido, Gifu 501-1193, Japan*

Correspondence should be addressed to Tomohiro Itoh; titoh@bio.mie-u.ac.jp

Received 15 November 2022; Revised 29 May 2023; Accepted 7 June 2023; Published 26 June 2023

Academic Editor: Ioannis D. Bassukas

Extracellular vesicles (EVs) secreted from adipose-derived stem cells (ADSCs) are known to exhibit collagen synthesis and migration activity in fibroblasts. These EVs can be used as a regenerative medicine and for cosmetic medicinal materials. Royal jelly (RJ) is produced from the hypopharyngeal and mandibular glands of honeybees (nurse bee), which contains apicin and 10-hydroxy-2-decenoic acid, compounds that promote fibroblast proliferation and collagen and elastin synthesis. Here, we investigated whether RJ could further enhance the physiological function of ADSC-EVs on fibroblasts. The findings confirmed that lyophilized RJ and enzyme-treated RJ enhanced the secretion of EVs by ADSCs, increasing the proliferation, migration, and collagen synthesis of fibroblasts compared to those induced by conventional ADSC-EVs. Bioinformatics analysis was conducted using various software programs, based on the data obtained from comprehensive gene expression and small RNA profiling analyses through next-generation sequencing; the results suggested that the RJ treatment of ADSC-EVs significantly enhanced the expression of genes related to extracellular matrix composition. Our findings suggest that the ADSC-EVs qualitatively altered using RJ could offer a more effective therapeutic material for regenerative and cosmetic medicine than conventional ADSCs-EVs.

1. Introduction

Recently, cells, the smallest units of the human body, have been found to secrete extracellular vesicles (EVs) and exosomes to communicate among each other and regulate biological functions, such as proliferation and differentiation [1, 2]. In particular, during differentiation, the EV inclusion profile changes drastically, and the information prioritized by the cell to adapt to its environment is internalized and propagated to the receptor cells. Adipose tissue-derived stem cells (ADSCs) have been used for regenerative medicine treatments owing to their ability to differentiate into bone, cartilage, vascular endothelium, and nerve cells; additionally, they are a commonly accepted treatment for osteoarthritis [3, 4]. Accordingly, ADSCs not only are attracting attention in the field of regenerative medicine but also in cosmetology, as they promote fibroblast migration and collagen production in skin wounds and increase the expression of enzymes that inhibit other enzymes from degrading collagen, a primary substance contributing to skin elasticity [5–7]. EVs and/or exosomes secreted by ADSCs are also currently attracting attention as structures that regulate

many biological processes in target cells, such as attenuating inflammation and obesity, in addition to promoting skin cell differentiation [8–11]. ADSCs-EVs and/or exosomes have shown remarkable therapeutic effects, such as ameliorating a hepatic fibrosis in tetrachloride-induced liver cirrhosis mice, improving a wound closure and angiogenesis in diabetic mice, and preventing frailty, improving health span, and decreasing epigenetic age in elderly mice; therefore, these EVs and/or exosomes have the potential to contribute to the medicinal efficiency across various diseases and biological function [12–15].

Honeybees are "social insects" whose society resembles that of humans and are established into regular groups. That is, the queen bee is in charge of egg-laying, the worker (nurse) bees command labor, and the male bees are responsible for mating. All female bee larvae receive an abundance of royal jelly (RJ) approximately for the first 3 days; thereafter, only the larva that continues to be provided RJ becomes the queen. Specifically, nurse bees digest pollen in the hypopharyngeal and mandibular glands to secrete RJ, a yellowish-white creamy liquid. Sugiyama et al. [16] reported that RJ primarily consists of 60%–70% moisture, 9–18% proteins, 7–18% carbohydrates, and 3–8% lipids. Lercker et al. [17] also reported that ~ 95% of the RJ lipid content includes free fatty acids, with 10-hydroxy-trans-2-decenoic acid (10H2DA) and 10-hydroxydecanoic acid (10HDAAA) accounting for nearly 80%. RJ is also rich in other components, such as free amino acids, vitamins (biotin, thiamine, niacin folic acid, inositol, riboflavin, pyridoxine, vitamin A, C, D, and E), and minerals (calcium, copper, sodium, potassium, zinc, iron, and manganese) [18, 19]. The queen bee that continues to ingest RJ receives many benefits, including growing to a size greater than that of the worker bees, developing reproductive organs, and having a prolonged lifetime. Therefore, RJ is thought to contain numerous beneficial components and has been reported to display various pharmacological effects when ingested by humans. In particular, *in vitro* and *in vivo* studies using these case models have shown that RJ has beneficial effects on reproductive health (antioxidant, hormone balance control, premenstrual syndrome reproduction effects, and being useful for postmenopausal treatment), neurodegenerative and aging diseases (promoting longevity and used for Alzheimer's and mental health treatments), and skin care and wound healing (collagen production, anti-photoaging, fibroblast migration, and vasodilatation); further, it expresses immunomodulatory activity [20–25].

The present study focused on the functional promotion of skin cells, such as keratinocytes and fibroblasts, by ADSCs-EVs treated with RJ, and investigated the effects of the RJ-treated ADSC-EVs on the migration ability and collagen production of fibroblasts. The findings demonstrated that RJ enhances EV production from ADSCs and significantly induced proliferative as well as migratory effects and collagen production in normal human dermal fibroblasts without obvious cytotoxicity. This represents the first report to show that RJ can be a candidate material for promoting ADSC-EV secretion and skin care function.

2. Methods

2.1. Materials

2.1.1. Preparation of Freeze-Dried RJ and Enzyme-Treated RJ. Raw RJ (rRJ) was obtained from beekeepers (Zhejiang Sheng, China) and stored at −20°C, whereas non-protease-treated RJ (nRJ) was obtained via lyophilizing rRJ and protease-treated RJ (pRJ) was obtained as described in previous research [26]. All RJ samples were prepared by Yamada Bee Company, Inc. (Okayama, Japan), and standardized using certain the amounts of specific fatty acids: 10H2DA and 10HDAAA.

10H2DA was purchased from Hangzhou Eastbiopharm, Co., Ltd. (Hangzhou, China), and 10HDAA was purchased from Combi-Blocks, Inc. (San Diego, CA, USA). 2-Decenedioic acid (2DA) was purchased from Sundia MediTech Co., Ltd. (Shanghai, China), and sebacic acid was purchased from Sigma-Aldrich Co., LLC. (St. Louis, MO, USA).

2.1.2. Cell Culture. ADSCs (code#PT5006) and normal human fibroblasts (NHDFs) (code#CC-2511) were obtained from Lonza (Tsukuba, Ibaraki, Japan). Cells were cultured in a humidified atmosphere at 37°C with 5% CO_2 in ADSC growth medium BulletKit™ (Lonza, code#PT4505) and FGM™-2 Fibroblast growth medium-2 BulletKit™ (Lonza, code#CC3132), respectively.

2.2. Purification of EVs Derived from the ADSC-Cultured Media. ADSCs were seeded in a T75 flask (Thermo Fisher Scientific Inc., MA, USA) at a density of 1×10^5 cells/mL and precultured for 48 h. The cells were further independently cultured for 5 days in an ADSC medium containing each type of RJ (final concentration, 200 μg/mL). After 5 days, the cultured media were collected into a sterilized 50 mL tube and stored at 4°C until the EV isolation. Fresh cultured medium (CM) was added to cells and cultured for an additional 5 days. Subsequently, the culture media were collected again and combined with the previously collected media. The resulting supernatant was centrifuged at 15,700 × g for 30 min at 4°C to remove cells and other debris. The supernatants were collected and subjected to size exclusion chromatography (qEV70 nm, Meiwafosis Co., Ltd., Tokyo, Japan). Then, aliquots were ultracentrifuged at 419,250 × g for 1 h at 4°C. Without disturbing the EV pellet, the supernatant was carefully removed using a sterilized Pasteur pipette. EVs were resuspended in phosphate-buffered saline (PBS). The protein levels of the EVs samples were quantified using the BCA method (Thermo Fisher Scientific Inc.).

2.3. Nano Tracking Analysis (NTA). The purified EV particle count and size distribution were measured using a NanoSight LM10 instrument (NanoSight, Wiltshire, UK). The collected EV pellet was suspended in PBS (1 mL) and then diluted to 1 : 100 in PBS before the analysis. NTA (NanoSight, version 2.3) was used to capture and analyze the data.

2.4. Scanning Electron Microscopic Observation. The isolated ADSC-EV pellets suspended in PBS were fixed in 1.25% (v/v) glutaraldehyde (pH 7.4) for 15 min and then placed on 3 μm polyethylene beads (White Estapor Microspheres, Merck Chimie SAS, Lyon, France) coated with poly-L-lysine. Specimens were rinsed in PBS, post-fixed in 1% (v/v) osmium tetroxide (pH 7.4) for 20 min, and dehydrated using a graded ethanol series. Subsequently, the samples were coated with platinum-palladium and observed using scanning electron microscopy (SEM, Hitachi S-5000; Hitachi, Tokyo, Japan).

2.5. Transmission Electron Microscopic Observation. The isolated ADSC-EV pellets were fixed in 2.5% (v/v) glutaraldehyde (pH 7.4) for 40 min, fixed in 1% (v/v) osmium tetroxide (pH 7.4) for 40 min, and dehydrated in a graded ethanol series. After dehydration, the samples were embedded in an epoxy resin mixture, polymerized, cut into 70 nm sections, and then observed using transmission electron microscopy (TEM, Hitachi H-7100 and H-7650 instruments, Hitachi).

2.6. Western Blotting. The EVs of each type were resuspended in a radioimmunoprecipitation assay buffer containing protease (25 × Complete®) and phosphatase inhibitors (Sigma-Aldrich). Their protein content was measured using a DC protein assay kit (Bio-Rad, Hercules, CA, USA). Each whole cell lysate was resuspended in sodium dodecyl sulfate (SDS)-polyacrylamide gel electrophoresis (PAGE) buffer containing 2% mercaptoethanol and boiled at 98°C for 5 min. Protein samples were subjected to SDS-PAGE and subsequently electroblotted onto polyvinylidene difluoride (PVDF) membranes (GE Healthcare, Pittsburgh, PA, USA). After blocking the non-specific binding sites for 1 h using 5% (w/v) non-fat milk (Becton Dickinson and Co., Sparks, MD, USA) in tris-buffered saline containing 0.1% Tween 20 (TBST), each membrane was incubated overnight at 4°C with the various primary antibodies. Each membrane was then washed three times in TBST, incubated further with a horseradish peroxidase-conjugated secondary antibody at room temperature (22 ± 2°C), and then washed again three times in TBST. Protein bands were detected using an enhanced chemiluminescence kit (GE Healthcare) and chemiluminescence detector (iBright FL1500 Imaging System, Thermo Fisher Scientific Inc.).

2.7. PKH67 Labeling of EVs In Vitro. Purified EVs were labeled with the green fluorescent membrane marker Paul Karl Horan (PKH) 67 dye according to the manufacturer's instructions. In brief, EVs were suspended in diluent C (250 μL), to which PKH67 (1 μL) was added, followed by incubation for 5 min. The labeling process was stopped by adding an equal volume of NHDF growth medium to 1% exosome-free fetal bovine serum (FBS), followed by incubation for 1 min. NHDFs were seeded on a LAB-TEK® II chamber slide (Thermo Fisher Scientific Inc.) at a density of 2×10^5 cells/mL and precultured for 24 h; thereafter, the labeled EVs were added to NHDFs and incubated at 37°C for 24 h. The cellular uptake and exosome internalization were captured using an all-in-one fluorescent microscope BZ-X800 (Keyence Co., Osaka, Japan).

2.8. Cell Proliferation Assay. Cell survival rates were measured via a Premix WST-1 cell proliferation colorimetric assay system (Takara Bio Inc., Kusatsu, Shiga, Japan), according to manufacturer's instructions. In brief, ADSCs or NHDFs were seeded on a 96 multiple well plate at a density of 1×10^4 cells/mL and precultured for 24 h. Thereafter, the CM was replaced with ADSC or NHDF growth medium (100 μL) supplemented with each RJ type at different concentrations (100, 200, and 300 μg/mL) or EVs (final concentrations: 50, 200, and 400 ng protein/mL), and the cells were cultured for an additional 72 h. After treatment, the CM was replaced with 100 μL of ADSC or NHDF growth medium supplemented with WST-1 reagent, and the cells were again incubated in 5% CO_2 at 37°C for 2 h. The absorbance (Abs) was measured at 450 nm (reference 690 nm) using a plate reader (Varioskan LUX™ multimode microplate reader, Thermo Fisher Scientific Inc.), and the results shown represented the averages of three independent experiments. The cell viability percentage was calculated using the following equation:

$$\text{cell viability } (\%) = \frac{\text{Abs}_{450\,nm \text{ of sample-treated cells}} - \text{Abs}_{690\,nm \text{ of sample-treated cells}}}{\text{Abs}_{450\,nm \text{ of untreated cells}} - \text{Abs}_{690\,nm \text{ of untreated cells}}} \times 100. \quad (1)$$

2.9. Cell Migration Assay. NHDFs were seeded on a 12 multiple well plate at a density of 1×10^5 cells/mL and precultured for 24 h. Following the preculture for 24 h, each RJ (50, 100, and 200 μg/mL) or EVs (200 ng protein/mL) were added, respectively, to the culture media and cells were cultured for an additional 24 h. After confirming that 100% confluency had been reached, a linear wound was generated in the cell layer using a sterile 1,000 μL pipette tip, and the cellular debris was washed using PBS. Thereafter, CM was immediately added, and cells were incubated in 5% CO_2 at 37°C for 24 h. Three representative images of each well for the scratched area were captured using a microscope to estimate the migration ability of the NHDFs. The experiments were repeated three times, and the migration distance from the wound edge was analyzed using ImageJ.

2.10. Amount of Synthesized Intracellular Collagen. Collagen biosynthesis was measured by performing a colorimetric assay using the collagen quantitation kit (Cat. No. COL-001, Cosmo Bio Co., Ltd., Tokyo) developed by Yasmin et al. [27] for which the manufacturer's instructions required an enzymatic degradation and fluorescence (FL) reaction. NHDFs were seeded on a six multiple well plate at a density of 1×10^5 cells/mL and precultured for 24 h. After preincubation, each RJ (200 μg/mL) or EV (200 ng protein/mL) concentration was added, and the cells were incubated for 3 days. Then, fresh NHDF growth medium was added to cells, which were further cultured for 48 h. Subsequently, cells were washed twice with ice-cold PBS, and their intracellular collagen content was measured. The absolute collagen content was calculated from a standard curve prepared using a collagen standard solution (500 μg/mL) and normalized based on the viable cell number, which was determined using a Premix WST-1 cell proliferation assay system.

2.11. RNA Isolation, RNA-Seq, and Small RNA-Seq Analyses. Total RNA was extracted from the RJ-treated ADSCs and EVs prepared by using an RNeasy Mini Kit (Qiagen, Hilden, Germany). Corresponding RNA levels were measured using a NanoDrop 2000 spectrophotometer (Thermo Fisher Scientific Inc.). All RNA samples were subsequently analyzed using TapeStation or bioanalyzer (Agilent Technologies, Santa Clara, CA, USA) to confirm that the RNA integrity number was ≥9.0. The isolated RNA was stored at −80°C until the RNA-seq and small RNA-seq analyses. RNA library construction and Illumina sequencing were performed by Takara Bio Inc (Siga, Japan).

RNA samples were checked for degradation using a bioanalyzer (Agilent Technologies), and the libraries for the RNA-seq and small RNA-seq analyses were prepared using SMART-Seq® stranded kit and SMARTer® RNA unique dual index kits (both from Takara Bio). A QIAseq miRNA library kit and a QIAseq miRNA NGS 96 Index IL (both from Qiagen) were used to prepare libraries for the RNA-seq and small RNA-seq analyses, respectively. These libraries were then immediately sequenced using a NovaSeq 6000™ next-generation sequencer (Illumina; reagents: NovaSeq 6000 SP reagent kit, NovaSeq Xp 2-lLane kit; software: NovaSeq Control Software *v*.1.6.0, Real Time Analysis *v*.3.4.4, and bcl2fastq2 *v*.2.20). In total, 150 paired-end nucleotide sequences equivalent to 100 Gb/660 million reads per sample were acquired.

Differential gene expression analysis was processed using DRAGEN Bio-IT Platform *v*.3.6.3 (Illumina) according to the following steps. After mapping the read sequences obtained via sequence analysis to the genome sequence, the positional information engraved in the map was used to calculate the expression levels of each gene and transcript based on the gene definition file. Annotation information was added, and the expression levels were summarized. (Reference sequence file: GPCh38.primary_assembly.genome.fa.gz, site name: GENCODE, release: 35; Gene definition: gencode.v35.primary_assembly.annotation.gtf.gz, site name: GENCODE, release: 35).

For small RNA sequence analysis, the number of mature miRNAs and other non-coding RNAs was determined using CLC Genomics Workbench (Qiagen). Transcripts per million (TPM) values were then calculated and annotated using CLC Genomics Workbench v.20.0.4, Biomedical Genomics Analysis Plugin v.20.1.1, and Phyton v.3.6.8; using miRNA data files. Data.gz (obtained from: miRbase, release: 22.1), and Homo_sapiens. GRCh38.ncrna.fa.gz (obtained from: Ensembl, release: 102).

The datasets with TPM < 16 were considered data noise and excluded, while all the other values were log-transformed to calculate the normally distributed logTPM values. To determine the genes showing expression variations, the following sorting conditions were used: a $\log_2(\text{TPM}) \geq 2$ or $-2 \geq \log_2(\text{TPM})$, and a p value ≤0.05 for untreated ADSCs or ADSCs-derived EVs, respectively. For small RNA, the following sorting conditions were used: $\log_2(\text{TPM}) \geq 1$ or $-1 \geq \log_2(\text{TPM})$ for ADSCs or ADSCs-derived EVs, respectively, and a p value ≤0.05. Hierarchical clustering analysis was performed using MeV (https://mev.tm4.org3/welcome), a microarray analysis software program developed by the Dana-Farber Cancer Institute. Gene ontology (GO) analysis was performed using the following functional groups: biological process, cellular component, and molecular function, whereas Kyoto Encyclopedia of Genes and Genomes (KEGG) pathway enrichment analysis was performed using the Database for Annotation, Visualization, and Integrated Discovery (DAVID) web tool provided by the National Institute of Allergy and Infectious Diseases (https://David.ncifcrf.gov/). The GO terms were sorted based on the p values.

2.12. Quantitative Real-Time Polymerase Chain Reaction (qRT-PCR). To confirm the reproducibility of the miR-205-5p expression profile obtained from the small RNA-seq analysis, a TaqMan® miRNA reverse transcription and TaqMan® miRNA assay kit (Applied Biosystems, Waltham, MA, USA) was used. Following each RJ treatment for 72 h, the total RNA was extracted from cells and EVs using TRIzol containing phenol/guanidinium isothiocyanate and a DNase I treatment. Complementary DNA (cDNA) was then synthesized using reverse transcriptase and the total RNA (50 ng). The products were subjected to qRT-PCR using an Applied Biosystems StepOne™ RT-PCR system. The expression levels were normalized to those of U6B small nuclear RNA (RNU6B), which was used as the internal control, and quantified using the comparative Ct (ΔΔCt) method. qRT-PCR consisted of 40 cycles at 95°C for 15 s and 60°C for 60 s, after an initial denaturation step at 95°C for 10 min.

2.13. Transfection of NHDF Cells with miRNAs. NHDFs were seeded into six-well plates at density of 1×10^5 cells/mL the day before transfection. The cells were transfected with microRNA-205-5p antisense inhibitor (Anti-miR-205-5p, final conc.; 40 nM, Applied Biosystems) using cationic liposomes (Lipofectamine RNAiMAX, Thermo Fisher Scientific Inc.) according to the manufacturer's protocol. The

transfection efficiency was >80% as evaluated by transfecting the cells with Alexa 488-conjugated dextran probe. Non-specific miRNA (Applied Biosystems) was used as control to determine non-specific effects. The cells were cultured in medium containing 10% FBS, 100 units/mL penicillin, and 100 μg/mL streptomycin which was changed at 12 h after the transfection. Transfected cells were then recultured for 1 day and then subjected to collagen biosynthesis assay.

2.14. Statistical Analyses. All data were analyzed using the statistical analysis software package for Macintosh, *v*.2.0 (Esumi, Tokyo, Japan). All data were expressed as means ± standard errors. Statistical significance among many groups was performed using the Tukey–Kramer test, and differences were considered significant at $p < 0.05$.

3. Results

3.1. Changes in Cell Proliferation, Cell Migration, and Collagen Synthesis for NHDFs Treated with rRJ, nRJ, or pRJ. The effect of each RJ type at different concentrations on fibroblast proliferation was first examined after 72 h using a WST-1 assay. The growth of cells treated with rRJ or nRJ was unchanged from that of non-treatment cells (Figure 1(a)). Comparatively, the proliferation of cells treated with 100 μg/mL of pRJ increased significantly, by approximately 40%; however, their growth decreased with increasing treatment concentrations. Notably, cell migration is a crucial function in the wound healing process; thus, the cell migration potency was examined using the normal human fibroblasts (NHDFs) through a scratch assay. The wound closure of cells treated with rRJ or nRJ was significantly increased for the treatments with concentrations >100 μg/mL (approximately 30%–38%), whereas no activity was detected in cells treated with pRJ across all concentrations for 24 h (Figure 1(b)). The results of an enhanced cell proliferation and migration activity obtained here are similar to those reported previously.

The intracellular collagen content in cells treated with rRJ, nRJ, or pRJ was further measured after 72 h using a collagen quantitation kit; however, the intracellular collagen content in cells treated with each RJ type was similar to that of non-treated NHDFs (Figure 1(c)).

3.2. Characterization of EVs Prepared from ADSC, nRJ-ADSC, and pRJ-ADSC Culture Medium. To disclose the characteristics of the EVs prepared from ADSC, nRJ-ADSC, or pRJ-ADSC cultured medium (CM), the particle size distribution and count were first analyzed using NanoSight. EV size was 93 ± 41, 71 ± 41, and 105 ± 71 nm in ADSC, nRJ-ADSC, and pRJ-ADSC CM, respectively (Figure 2(a)). The EV concentration in nRJ-ADSC CM was 2.01×10^8 particles/mL, ~50 times the EV concentration in ADSC CM (4.05×10^6 particles/mL). Conversely, the EV concentration in pRJ-ADSC CM was 2.22×10^7 particles/mL, nearly 5 times higher than that in ADSC CM, although lower than that of nRJ-ADSC CM (Figure 2(b)). The proliferation of ADSCs was not concentration-dependent for the various RJ treatments but increased by 30% (Figure 2(c)). These results suggest that the freezing, drying, and enzymatic treatments of RJ did not affect ADSC proliferation. The morphology of the ADSCs treated with RJ and the prepared EVs was further observed using SEM and TEM, which revealed the presence of more multivesicular bodies intracellularly in RJ-treated ADSCs than in untreated ADSCs (Figure 2(d), arrowhead). Moreover, a marked swelling of the endoplasmic reticulum was observed in RJ-treated ADSCs (Figure 2(d), arrow). The EVs prepared from either RJ-treated or untreated ADSC CM were spherical, primarily ranging from 50 to 200 nm in diameter (Figure 2(e)); however, TEM observations showed that the EVs prepared from ADSC CM were single vesicles, while those prepared from RJ-treated ADSC CM were multiple vesicles assembled to form a structure of EVs encapsulated in a substance that is likely an RJ-derived component (Figure 2(e), lower panel). The protein expression profiles of EV markers were further investigated in isolated ADSC, nRJ-ADSC, or pRJ-ADSC-EVs using western blotting. The EV markers Alix and CD9 were detected in all EVs, while CD9 was detected in all the cell lysate samples. However, GM130, a negative EV marker, was not detected in any of the EVs samples. This result indicates that there was no cell component contamination in the EVs prepared (Figure 2(f); Supplementary Figure 2). Additionally, when each PKH67 fluorescent-labeled EVs was exposed to NHDFs for 24 h, several EVs were taken up by cells. Based on the three-dimensional analysis, each incorporated EV was localized in the cytoplasm and primarily observed around the nucleus (Figure 2(g); Supplementary Figure 3, visualized as a green fluorescent dot in the microscopic observation image).

3.3. Changes in Cell Proliferation, Cell Migration, and Collagen Synthesis in NHDFs Treated with EVs Isolated from ADSC, nRJ-ADSC, or pRJ-ADSC CM. We further examined whether each EV could influence cell proliferation, cell migration, and collagen synthesis of NHDFs. Each EV treatment increased the cell proliferation of ADSCs by ~50% at a concentration of 400 ng protein/mL (Figure 3(a)). Further, the wound closure values of cells treated with the EVs were significantly increased in a dose-dependent manner (Figure 3(b)). The migration ability of cells treated with 400 ng protein/mL EVs was significantly higher than that of cells treated with EVs prepared from both RJ-treated ADSCs from conventional ADSCs. The intracellular collagen synthesis was significantly higher (~1.5-fold increase) in cells treated with EVs derived from both RJ-treated ADSC types but was virtually unchanged in cells treated with the EVs derived from untreated ADSCs (Figure 3(c)).

3.4. Differential Expression Profiles and Bioinformatics Analysis of ADSCs, nRJ-ADSCs, and pRJ-ADSCs or ADSC-EVs, nRJ-ADSC-EVs, and pRJ-ADSC-EVs. The ADSC growth levels and the amount of secreted EVs were altered, suggesting that the gene expression profile of ADSCs was significantly influenced by the RJ treatments. To analyze the

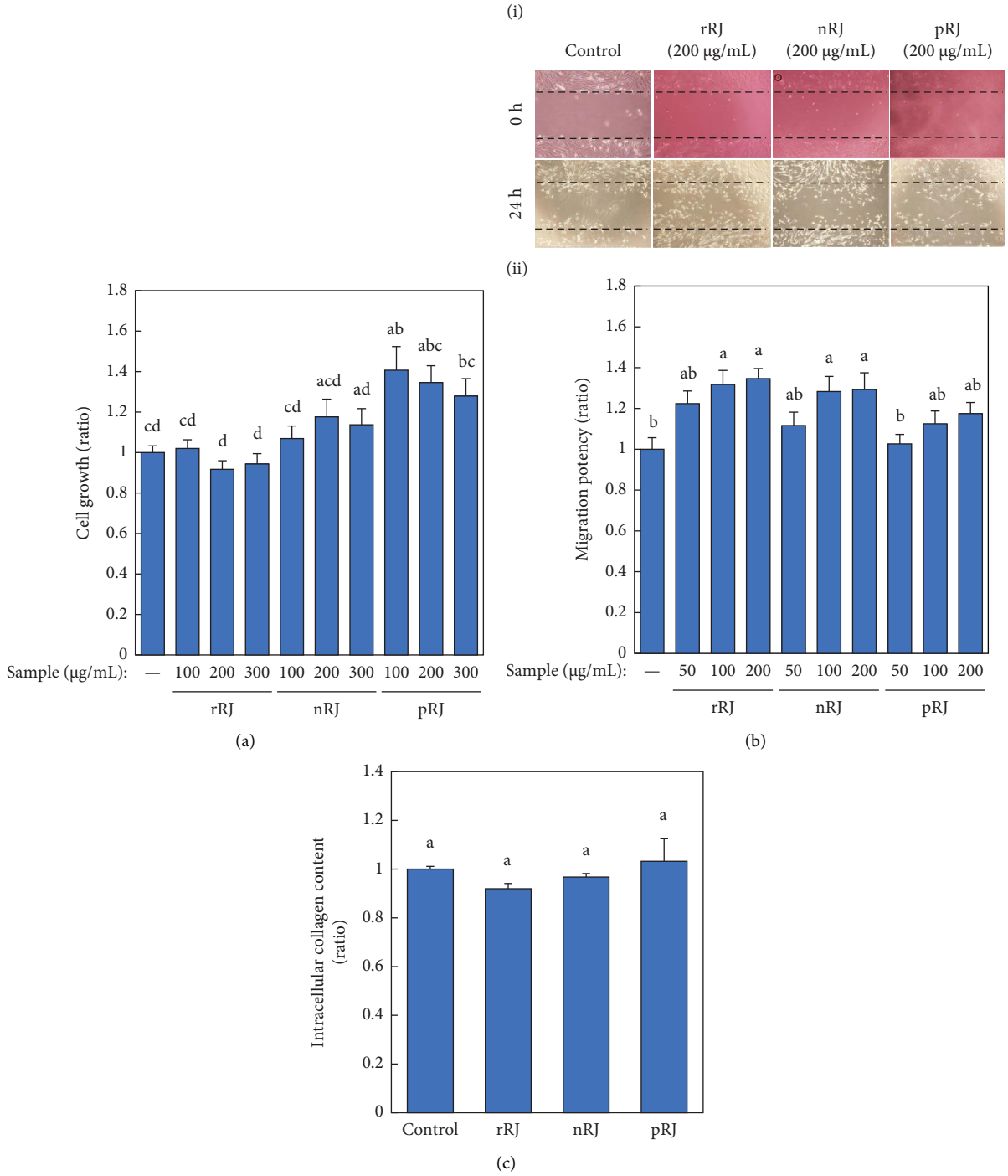

Figure 1: Influence of royal jelly (RJ) on cell physiology of normal human dermal fibroblasts (NHDFs). (a) Proliferation of each RJ-treated NHDF was measured by WST-1 assay. NHDFs were seeded in 96-well plates and allowed to attach for 24 h. NHDFs were then treated with the indicated concentrations of each RJ sample for 48 h ($n = 12$). Cell growth was measured using a spectrophotometer at 450 nm (reference: 690 nm). (b) Cell migration assay was performed for 24 h on each RJ-treated NHDF after scratching. (i) Microscopical images representing the *in vitro* cell migration potency of each RJ-treated NHDF. NHDFs were incubated in the presence or absence of each RJ, and images were captured at 24 h. (ii) Quantitative analysis of NHDF migration potency treated with each RJ ($n = 6$). (c) Comparison of type I collagen synthesis in NHDFs without treatment (control) and after 72 h of exposure to each RJ (all RJ sample final concentrations = 200 μg/mL). Data are presented as means ± SE. Statistical analysis was performed using the Tukey–Kramer test, and differences were considered significant for p values <0.05.

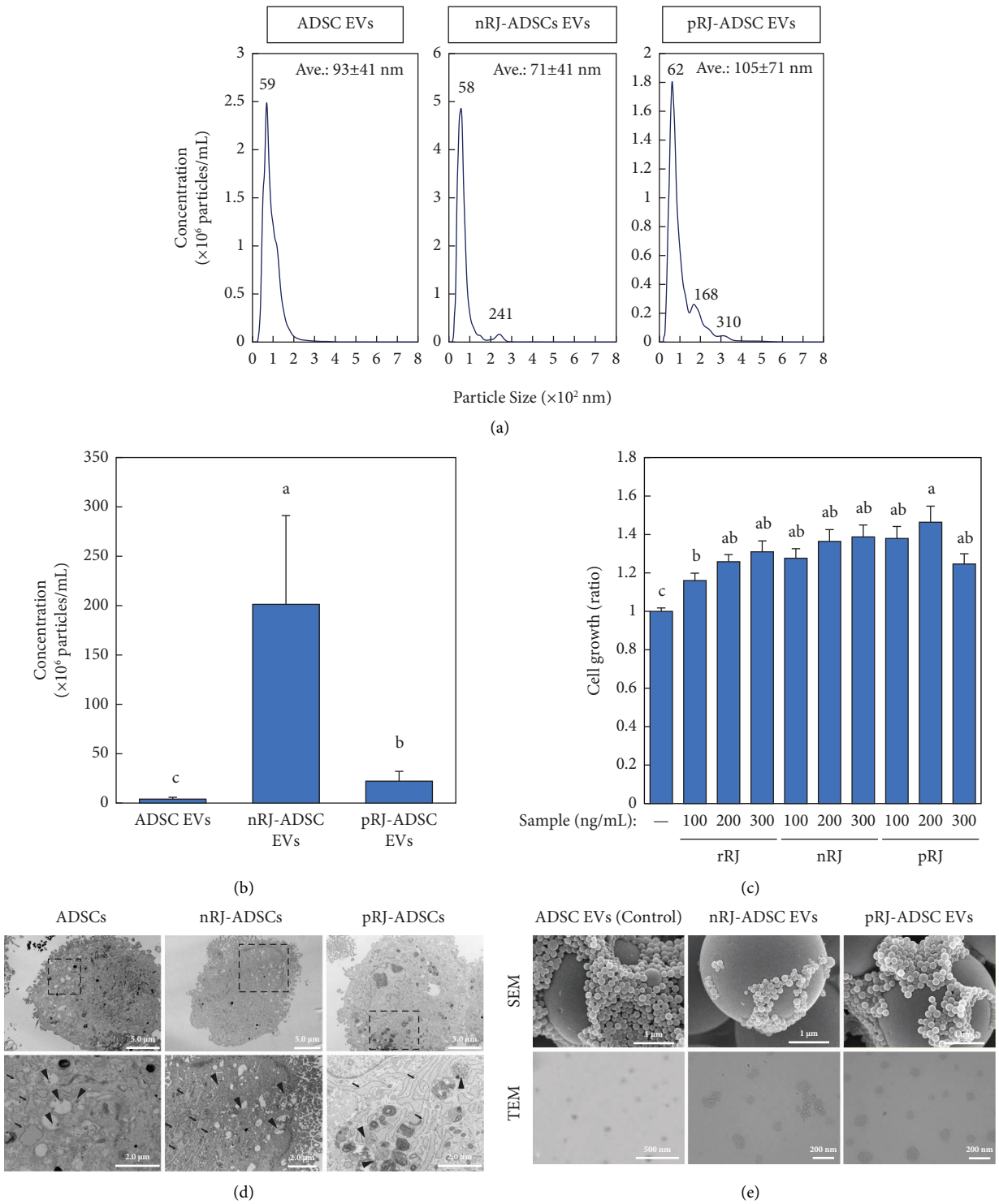

Figure 2: Continued.

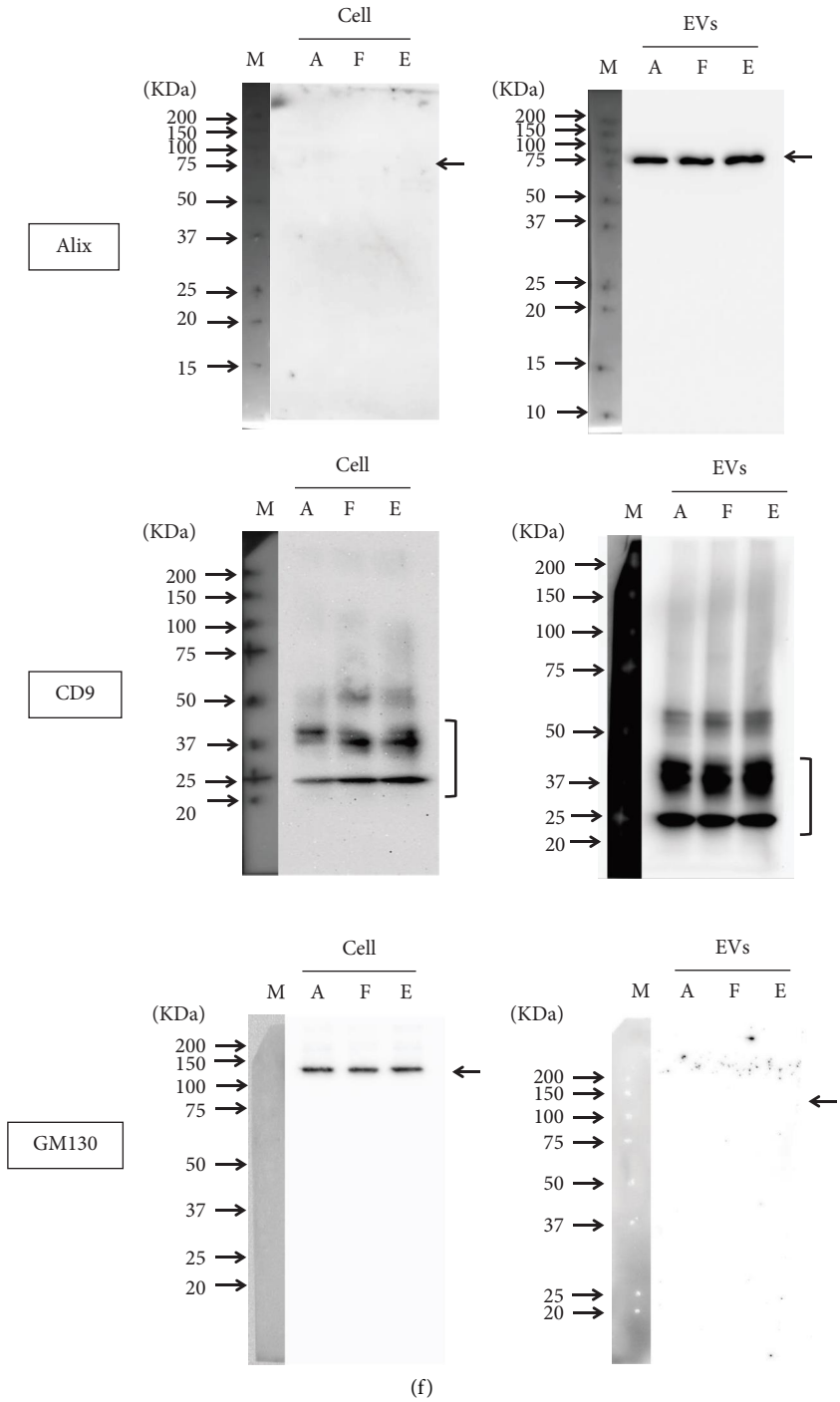

(f)

Figure 2: Continued.

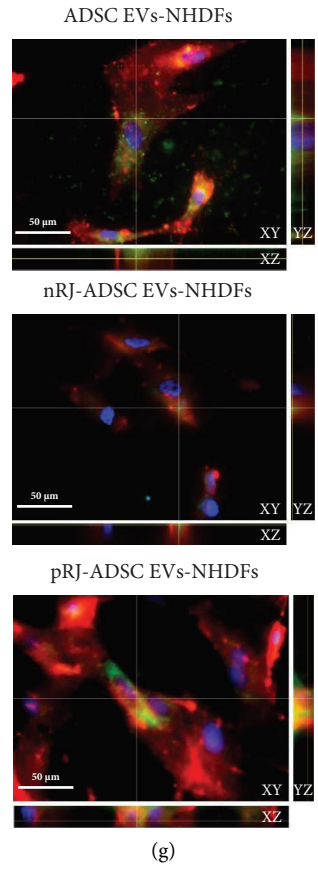

(g)

Figure 2: Morphological characterization of extracellular vesicles (EVs) prepared from ADSCs or ADSCs treated with royal jelly. (a) Particle distribution of ADSC-EVs, nRJ-ADSC-EVs, and pRJ-ADSC-EVs measured by nanoparticle tracking analysis. (b) Particle concentration of ADSC-EVs, nRJ-ADSC-EVs, and pRJ-ADSC-EVs was detected by NTA ($n = 5$). (c) Proliferation of each RJ-treated ADSC was measured by WST-1 assay. ADSCs were seeded in 96-well plates and were allowed to attach for 24 h. ADSCs were then treated with the indicated concentrations of each RJ sample for 48 h ($n = 12$). (d) Subcellular localization and size characterization of EVs in ADSCs treated with RJ examined by TEM. Each lower panel indicates enlarged area that is outlined in each upper panel. Multiple nanovesicles are encapsulated in multivesicular bodies. Arrowhead identifies multivesicular bodies or exosomes, whereas the arrow denotes the endoplasmic reticulum. (e) Representative SEM and TEM micrographs of prepared EVs. (f) Full-length western blot images for the exosomal protein (Alix, CD9) and non-exosomal protein makers (GM130): (A) ADSCs; (F) nRJ-ADSCs; (E) pRJ-ADSCs. (g) Uptake of each EV by NHDFs. NHDFs were exposed to each EV labeled with PKH67 (green) for 24 h. Arrows indicated PKH67-labeled EVs taken into NHDFs. Blue: nucleus stained with Hoechst33342. Red: cell membrane stained with CellROX™ Deep Red. Data are presented as means ± SE. Statistical analysis was performed using the Tukey–Kramer test, and differences were considered significant at $p < 0.05$.

differentially expressed genes (DEGs) among the three groups (ADSCs, nRJ-ADSCs, and pRJ-ADSCs, or ADSC-EVs, nRJ-ADSC-EVs, and pRJ-ADSC-EVs), RNA-seq and small RNA-seq analyses were performed, respectively.

Almost no genes in the nRJ- and pRJ-treated ADSCs whose concentration values changed significantly ($\log_2(\mathrm{TPM}) \geq 2$ or $-2 \geq \log_2(\mathrm{TPM})$) compared to that of untreated ADSCs were identified, rather, the only genes whose concentration was altered in nRJ- and pRJ-treated ADSCs were those encoding *IL-33* and *MED12L*, respectively. A majority of the other nucleotide sequences were snoRNAs and lncRNAs, types of non-coding RNAs present in the nucleolus. The sole gene that showed common variations in nRJ-ADSCs and pRJ-ADSCs was *SNORAC2* (Figure 4(a)). The number of genes with higher concentrations in nRJ-ADSC-EVs and pRJ-ADSC-EVs compared to ADSC-EVs was 1,950 and 1,525 genes, respectively (Figure 4(b)). A Venn diagram of the DEGs indicated that 721 genes (26.2%) were shared between the ADSC-EVs and nRJ-ADSC- EVs as well as between the ADSC-EVs, whereas 1,229 genes were shared between ADSC-EVs and nRJ-ADSC-EVs, and 804 genes were shared between ADSC-EVs and pRJ-ADSC-EVs. Conversely, the internal expression levels of 127 and 525 genes in nRJ-ADSC and pRJ-ADSC-EVs showed a decrease compared to those in ADSC-EVs, respectively, while 20 genes showed a common internal expression decrease (3.2%, Figure 4(b)). Supplementary Table 1 lists the top 20 genes whose internal expression increased or decreased in nRJ-ADSC-EVs and pRJ-ADSC-EVs compared to that of ADSC-EVs. Notably, the internal expression of various collagen genes was high in nRJ-ADSC and pRJ-ADSC-EVs (Figure 4(c)).

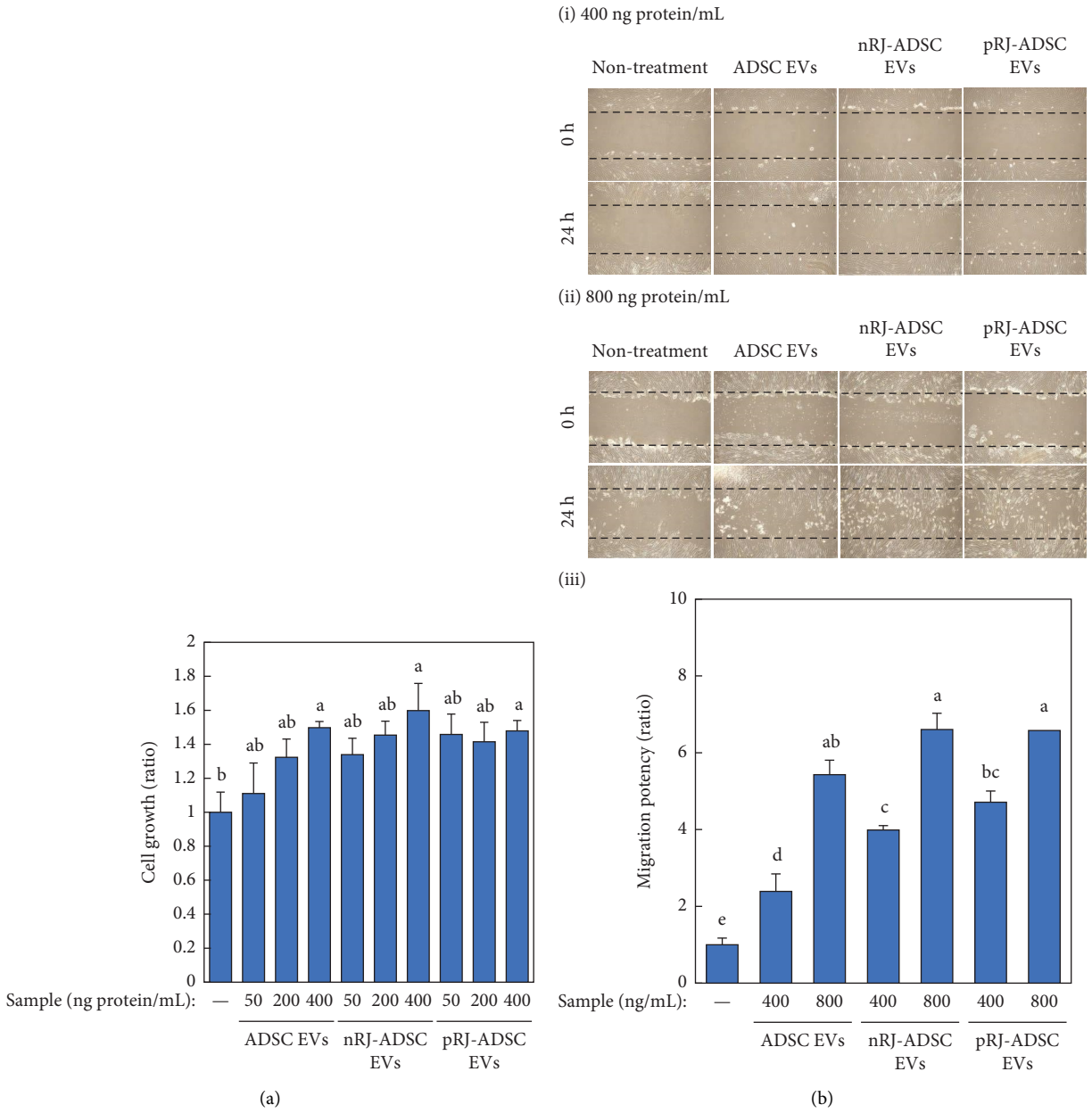

Figure 3: Continued.

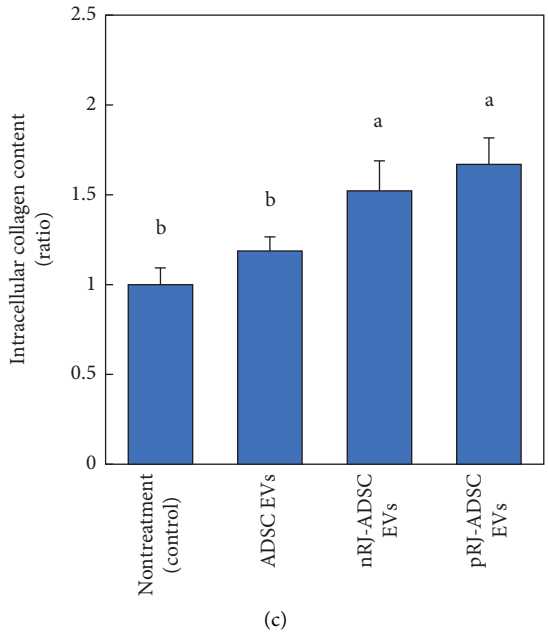

Figure 3: EVs prepared from RJ-treated ADSC culture medium promoted cell migration and collagen synthesis in NHDFs. (a) Proliferation of NHDFs treated with ADSC-EVs, nRJ-ADSC-EVs, and pRJ-ADSC-EVs was measured by WST-1 assay ($n = 12$). (b) Cell migration assay was performed for 24 h on each prepared EV NHDF after scratching. Microscopic images representing the *in vitro* cell migration potency of each RJ-treated NHDF: (i) EV concentration at 400 ng protein/mL, (ii) EV concentration at 800 ng protein/mL, and (iii) quantitative analysis of migration potency of NHDFs treated with each prepared EV ($n = 6$). (c) Comparison of type I collagen synthesis in NHDFs without treatment (control) and after 72 h of exposure to each prepared EV (all EV sample final concentrations were 200 ng protein/mL). Data are presented as means ± SE. Statistical analysis was performed using the Tukey–Kramer test, and differences were considered significant for $p < 0.05$.

To better understand the functions of the DEGs in the EVs isolated from RJ-treated ADSCs, gene ontology (GO) enrichment analysis was performed based on three functional groups: biological processes (BPs), cellular components (CCs), and molecular functions (MFs) (Figure 4(d); Supplementary Table 2). Within the BP functional group, the common upregulated DEGs were predominantly enriched in the extracellular matrix or extracellular structure organization (GO 0030198 and GO 0043062), collagen metabolic process (GO 0030199 and GO 0032963), and vasculature development (GO 0072359, GO 0072358, GO 0001944, and GO 0001568). Comparatively, within the CC function group, the common upregulated DEGs were predominantly enriched in the extracellular matrix (GO 0031012 and GO 0005578), endoplasmic reticulum system (GO 0005788 and GO 0005783), and cell membrane structure (GO 0070062, GO 0016020, GO 0009986, and GO 0005604). Lastly, within the MF functional group, the common upregulated DEGs were predominantly enriched in the extracellular matrix (GO 0005201). The KEGG pathway enrichment analysis was performed using the same analysis software tool. The KEGG enrichment results suggested that most of the genes were involved in the human papillomavirus infection, PI3K-Akt signaling pathway, and ECM-receptor interaction (Figure 4(e); Supplementary Table 3).

In the small RNA expression analysis, 159 (cell) or 57 (EVs) types of miRNAs were included in the analysis, in which the detected miRNAs with read count values < 16 were excluded due to noise. Hierarchical clustering analysis showed that both the ADSCs and secreted EVs could be classified into five clusters (Figure 5(a)). The miRNAs whose expression varied between the ADSCs and secreted EVs were extracted from each ADSC and secreted EV, as well as for each RJ treatment sample, while the common variable miRNAs were extracted as well. As a result, 64 and 27 miRNAs were commonly up- and downregulated in the ADSCs treated with each RJ sample compared to the corresponding levels in untreated ADSCs, respectively (Figure 5(b): Cell). Conversely, in the secreted EVs, the internalization levels of seven miRNAs, hsa-miR-335-5p, hsa-miR-130a-3p, hsa-miR-137-3p, hsa-miR-365a-3p, hsa-miR-205-5, hsa-miR-132-3, and hsa-miR-206, increased, while those of 17 miRNAs decreased (Figure 5(b): EVs). Only four ADSCs and secreted EVs showed similar expression changes upon treatment with each RJ sample: hsa-miRNA-205-5p (commonly increased), hsa-miRNA-141-3p, hsa-miRNA-191-5p, and hsa-miRNA-342-3p (commonly decreased).

3.5. Changes in miRNA-205-5p Expression and Sorting Levels in ADSCs and EVs by RJ Treatment. To confirm the levels of miRNA-205-5p in the ADSCs treated with RJ and in the EVs isolated from ADSCs treated with RJ, miRNA quantitative PCR amplification was performed. The miRNA-205-5p expression in ADSCs or EVs was significantly increased by

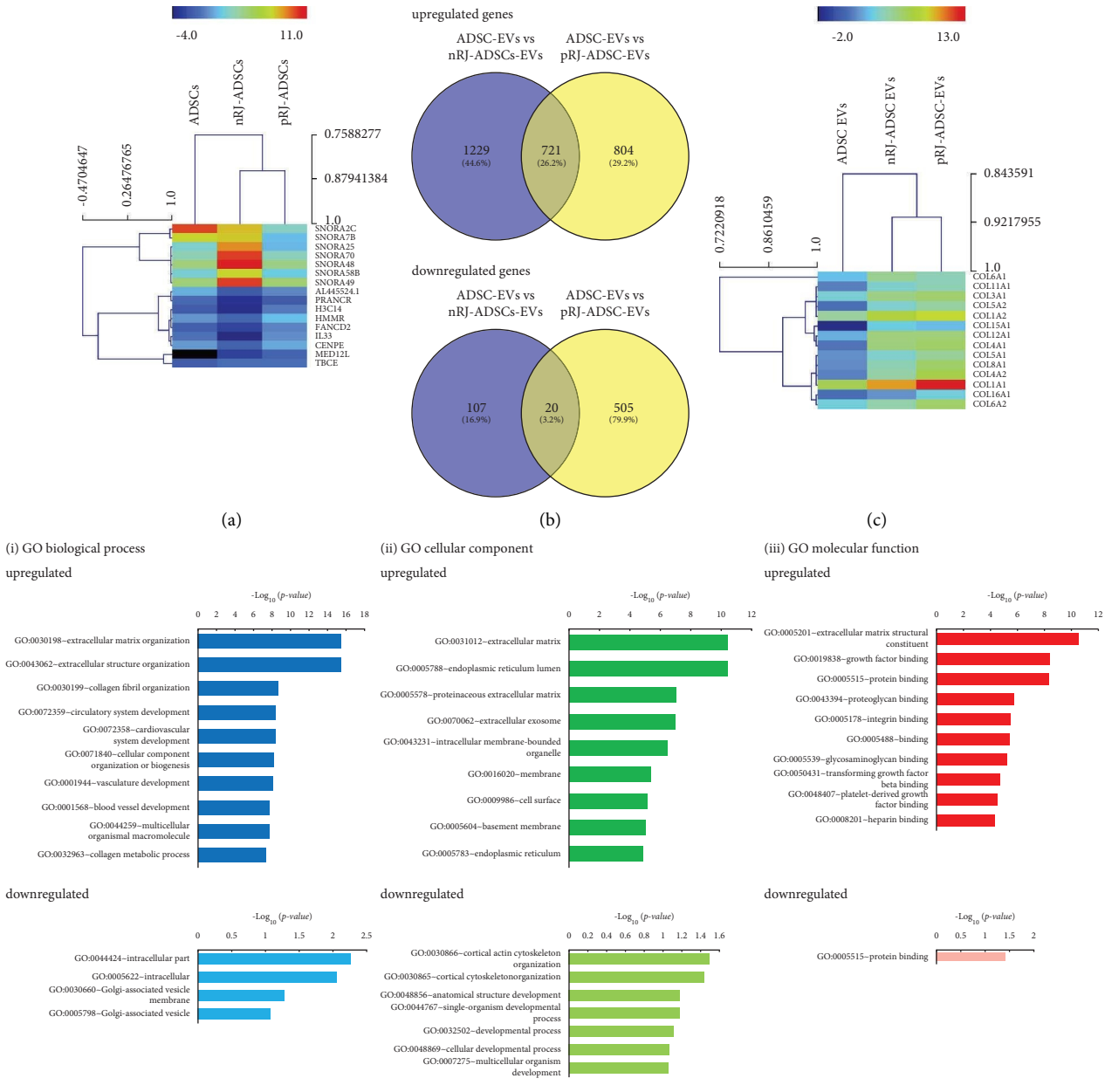

(a) (b) (c)

(d)

Figure 4: Continued.

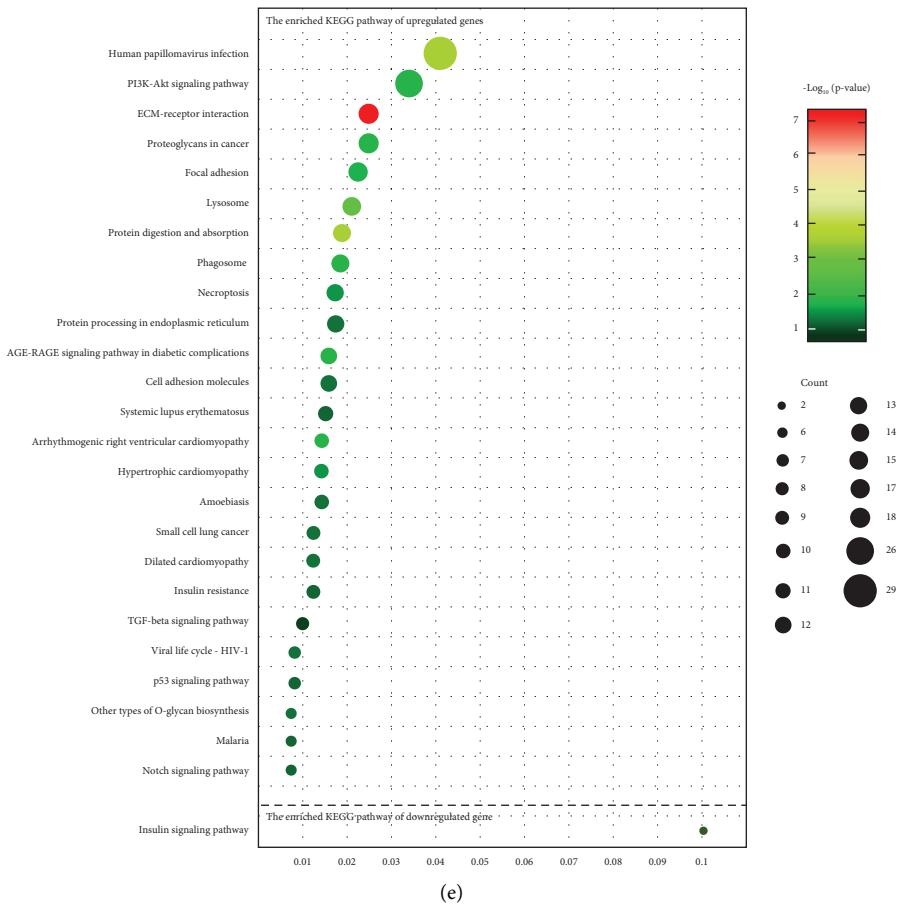

(e)

Figure 4: Differentially expressed transcript profiles of ADSCs treated with RJ and EVs isolated from ADSCs treated with RJ. (a) Hierarchical clustering analysis of differentially expressed genes in ADSCs treated with RJ. Rows and columns represent genes and samples, respectively, while legend depicts the Log_2FC of gene abundance where red and blue indicated high and low expression of DEGs, respectively. (b) Venn diagram of shared referenced genes between ADSC-EVs *vs.* nRJ-ADSC-EVs and ADSC-EVs *vs.* pRJ-ADSC-EVs. (c) Hierarchical cluster analysis and heat map visualization of known collagen family genes among the three groups: ADSC-EVs, nRJ-ADSC-EVs, and pRJ-ADSC-EVs. Rows and columns represented genes and samples, respectively, while legend represents Log_2FC of gene abundance where red and blue indicated high and low expression of DEGs, respectively. (d) Gene ontology enrichment analysis of up- and downregulated genes in EVs isolated from ADSCs treated with RJ. The top 10 GO enrichment terms are represented here: (i) biological process, (ii) cellular components, (iii) molecular functions, and (e) the KEGG enrichment analysis bubble diagrams of differentially expressed genes (DEGs) by DAVID.

RJ treatment compared to either that in ADSCs or in the EVs isolated from ADSCs (cells: ADSCs, 1.00 ± 0.06; nRJ-ADSCs, $2.35 \pm 0.30^*$; pRJ-ADSCs, $2.11 \pm 0.18^*$; EVs: ADSCs, 1.00 ± 0.03; nRJ-ADSCs, $2.85 \pm 0.29^*$; rRJ-ADSCs, $2.79 \pm 0.36^*$, $^*p < 0.05$, Figure 6(a)). We transfected fibroblasts with Anti-miR-205-5p and measured collagen level to further clarify the involvement of miRNA-205-5p in nRJ-ADSC-EVs and pRJ-ADSC-EVs induced collagen production. Transfection of Anti-miR-205-5p slightly suppressed nRJ-ADSC-EV and pRJ-ADSC-EVs-induced increase in intracellular collagen content (Figure 6(b)).

3.6. Secretion of ADSCs-EVs by Treatment with the Carboxylic and Dicarboxylic Acids in RJ. To identify the components involved in RJ production of EVs, we focused on fatty acids (decanoic and decenoic acids, decenoic diacid, and sebacic acid), which are unique to RJ and have been reported to maintain numerous different chemical activities. Next, EVs were prepared by adding these acids to ADSCs at concentrations of 200 μM. The particle size and concentration of each EVs were measured using NanoSight. Notably, the particle size was nearly identical among all EVs; however, no significant secretion-promoting effect was observed for either the carboxylic acid or the dicarboxylic acid treatments (Figure 7). In particular, EV production in cells treated with decenoic acid, decenoic diacid, and sebacic acid was approximately four-fold lower than that in untreated ADSCs.

4. Discussion

To investigate the role of RJ in the activation of skin fibroblasts by EVs secreted from ADSCs, the effects of RJ on the proliferation of ADSCs and NHDFs were first confirmed. It was found that RJ treatment enhanced the proliferation of ADSCs and NHDFs, as well as their ability to migrate to the

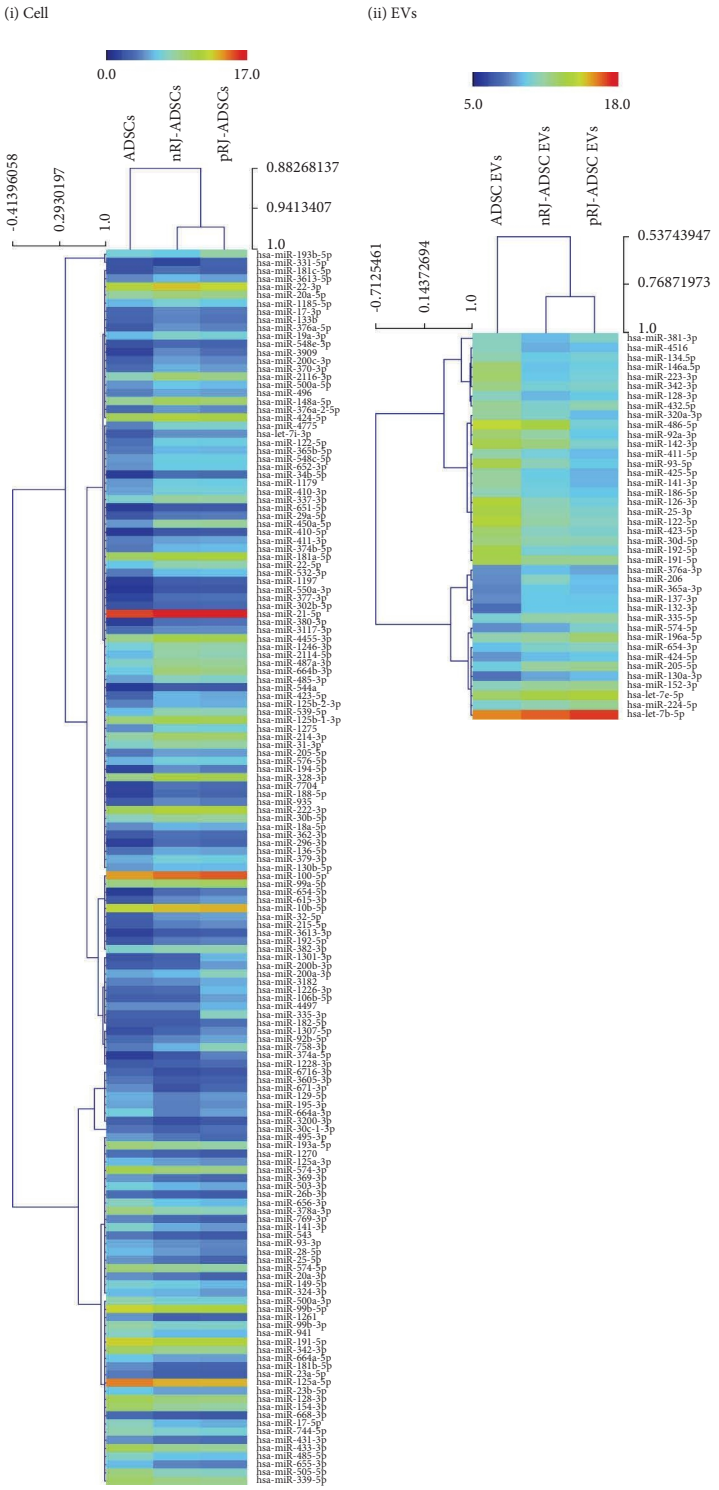

(a)

Figure 5: Continued.

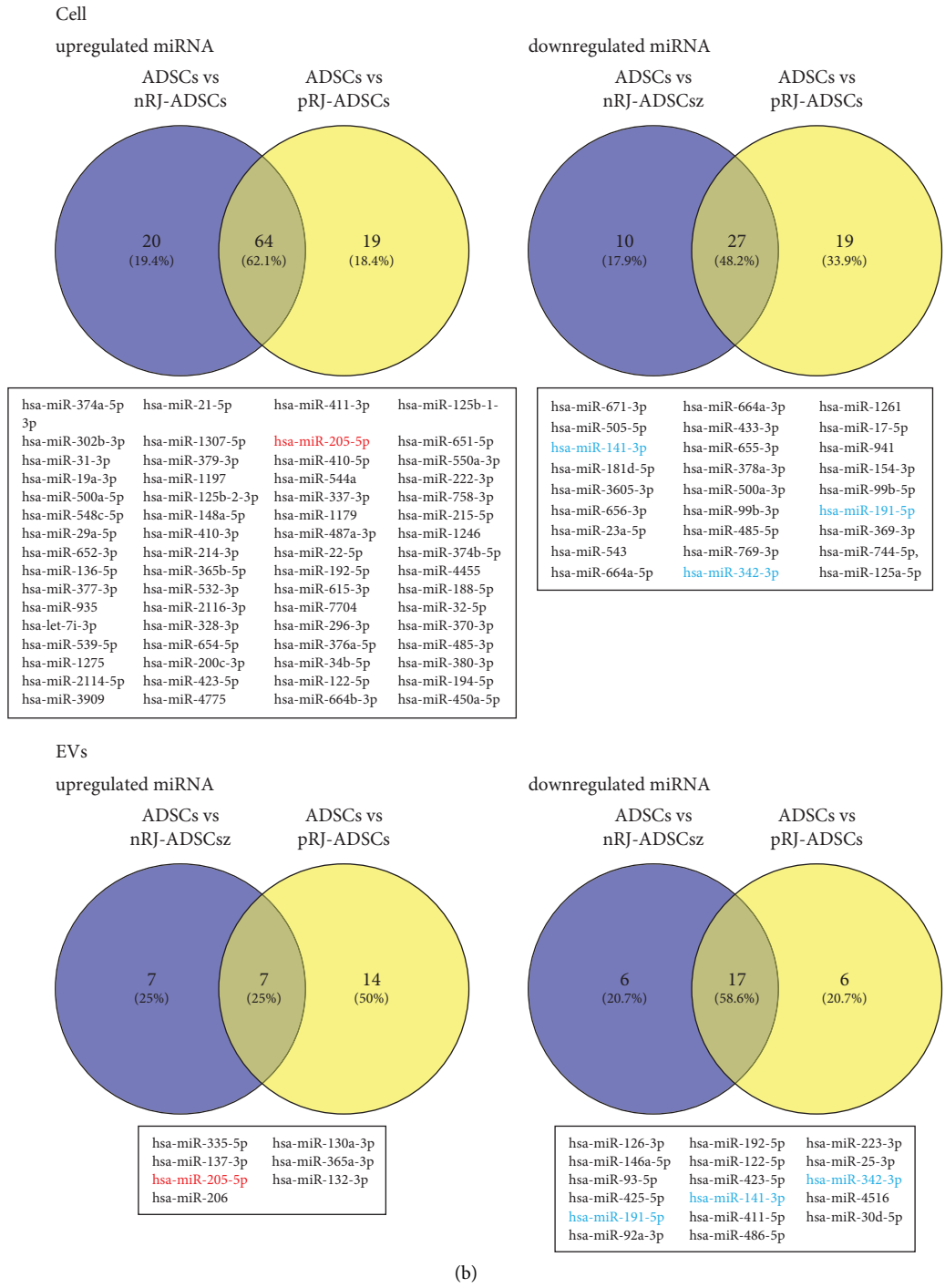

Figure 5: MicroRNA differential expression profiles in ADSCs treated with RJ and EVs isolated from ADSCs treated with RJ. (a) Differentially expressed miRNAs ($p < 0.05$) were analyzed by hierarchical clustering of the $\log_2$ value of each small RNA-seq signal in (i) ADSCs, nRJ-ADSCs, and pRJ-ADSCs or (ii) ADSC-EVs, nRJ-ADSC-EVs, and pRJ-ADSC-EVs. Relative changes in their expression are indicated by a color code, where red and blue indicate that the level of miRNA expression was higher or lower than the median value, respectively. (b) Venn diagram indicating the complete unique and shared expression patterns of miRNAs between ADSC-EVs *vs.* nRJ-ADSC-EVs and ADSC-EVs *vs.* pRJ-ADSC-EVs (left, upregulated miRNAs; right, downregulated miRNAs).

wound site; however, it had no significant effect on collagen production (Figures 1 and 2). Although RJ has been reported to contain apicin, a glycoprotein that stimulates collagen production, in addition to the fatty acid 10H2DA, the RJ used in this study did not induce collagen production in NHDFs. [28] Next, ADSCs were treated with RJ (nRJ and pRJ), and secretory EVs prepared via ultracentrifugation and size chromatography were examined for their effects on

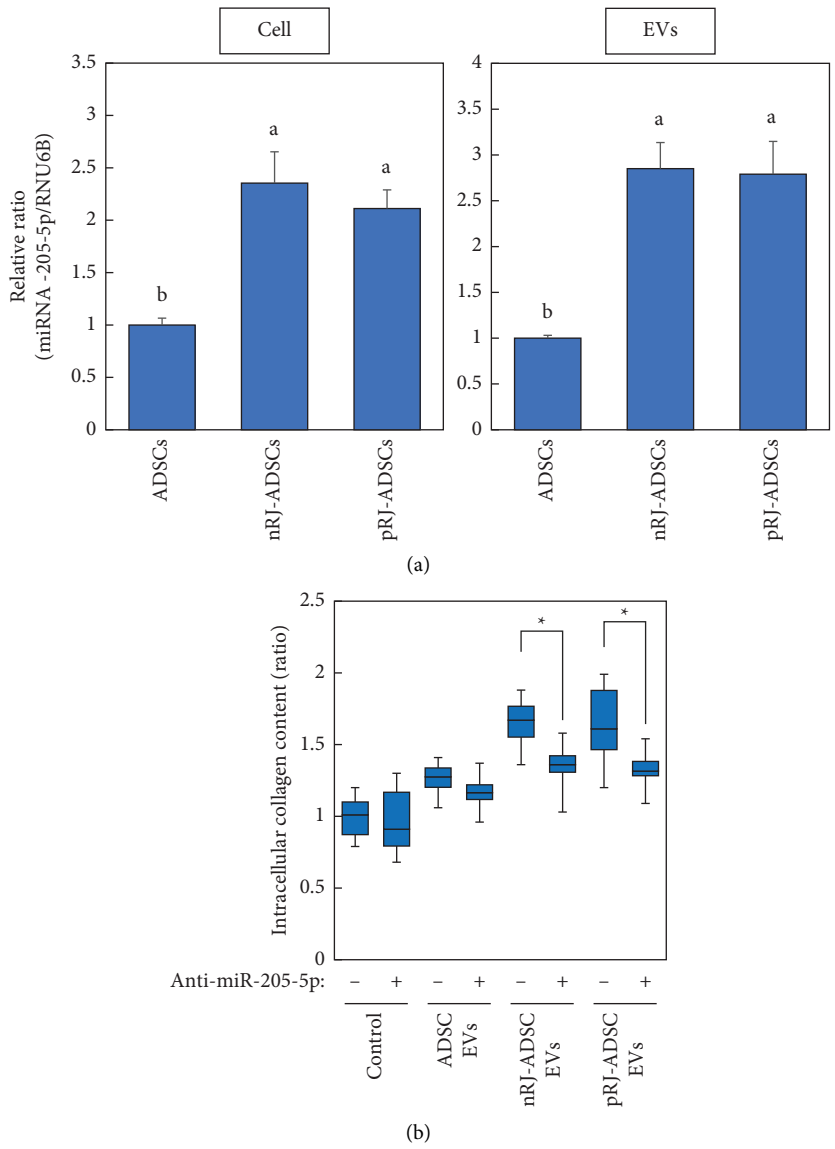

Figure 6: Changes in miRNA-205-5p expression and sorting levels in ADSCs and EVs due to RJ treatment and its effect on EV-induced collagen synthesis in miR-205-5p antisense inhibitor- (Anti-miR-205-5p-) transfected NHDF. (a) Changes of miRNA 205-5p expression (internalization or sorting) levels in ADSCs and prepared EVs treated with RJ. Following each RJ treatment for 72 h, total RNA was extracted from each cell and EVs by TRIzol containing phenol/guanidinium isothiocyanate with DNase I treatment. Expression (internalization) levels of miRNA 205-5p in each cells and EVs were analyzed via a TaqMan® miRNA reverse transcription and TaqMan® miRNA assay kit using the real-time polymerase chain reaction. Relative rations are shown with the values of non-treated ADSCs (designated as 1). Data are presented as means ± SE ($n = 6$). Statistical analysis was performed using the Tukey–Kramer test, and differences were considered significant at $p < 0.05$. (b) Effects of Anti-miRNA-205-5p on intracellular collagen synthesis in nRJ-ADSC-EVs and pRJ-ADSC-EVs stimulated NHDFs. The cells transfected with Anti-miR-205-5p significantly suppressed collagen synthesis following nRJ-ADSC-EVs or pRJ-ADSC-EVs stimulation. Relative ratios are shown with the values of non-treated ADSCs (designated as 1). Data are presented as means ± SE ($n = 9$). Statistical analysis was performed using Student's t-test, and differences were considered as statistically significant at $^{*}p < 0.05$.

NHDF growth, migration to the wound site, and collagen production. The particle sizes of the prepared EVs were relatively similar to those of the EVs secreted from untreated ADSCs for both RJ treatments, yet the particle concentrations increased by 5- to 50-fold after the RJ treatment. Both RJ-conditioned solutions (50 mg/mL) added to ADSCs contained $5–8.3 \times 10^5$ vesicles/mL; therefore, it was possible that the amount of RJ-derived EVs may be reflected in the measured EV concentration values. Nonetheless, considering that 40 μL of the RJ-conditioned solution was added to each 10 mL of medium, it was reasonable to assume that the RJ treatment promoted the secretion of EVs from ADSCs. Ramirez et al. [29, 30] reported that the exosome-like vesicles isolated from bee pollen, honey, and RJ exhibited antibacterial properties and pro-regenerative activity, while being incorporated into mammalian cells. The findings from

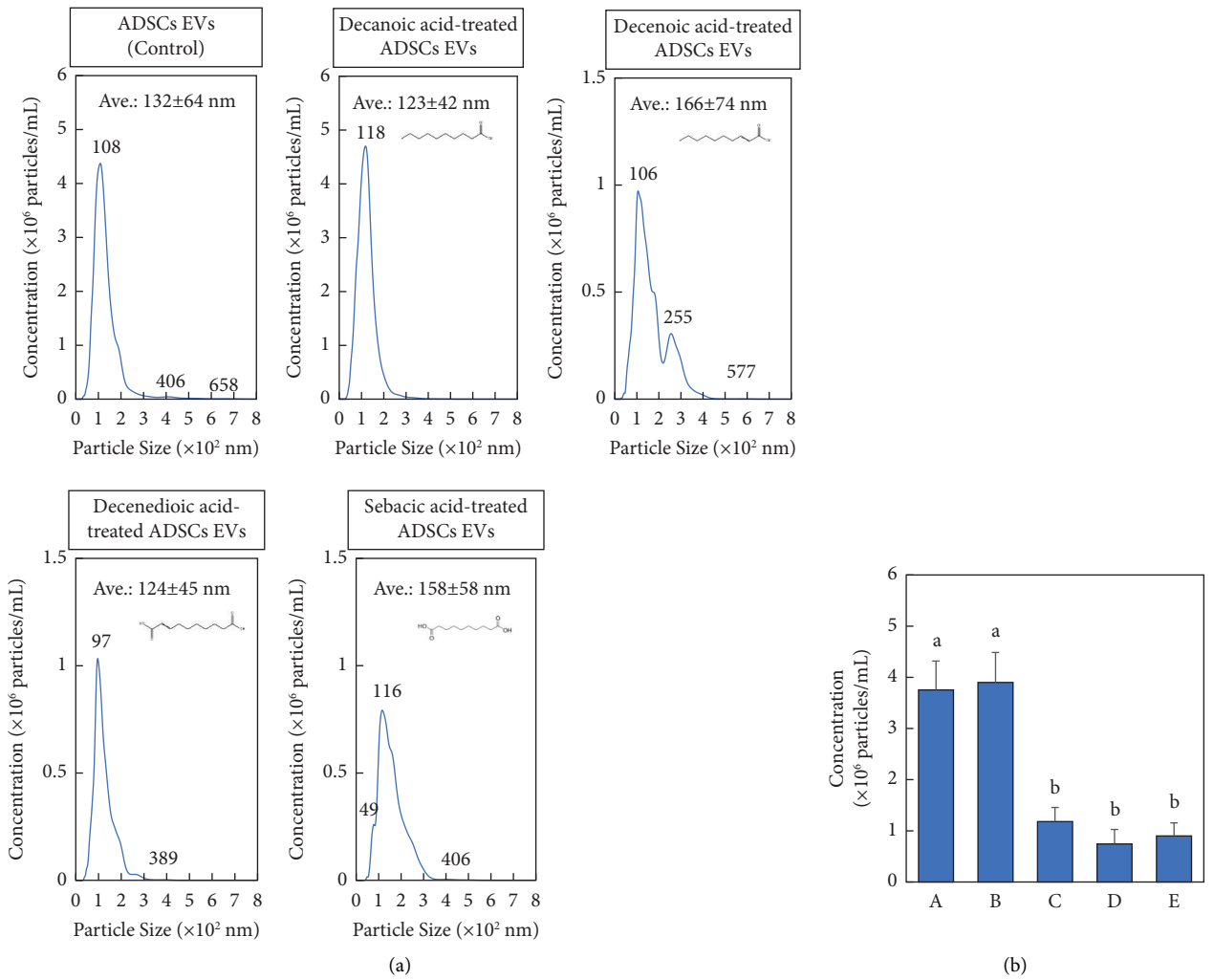

Figure 7: Free fatty acids in RJ did not alter secretion of extracellular vesicles from ADSCs. (a) Particle distribution and (b) particle concentration of prepared EVs isolated from ADSCs treated with free fatty acid components in RJ measured by NTA ($n = 5$). (A) ADSCs-EVs; (B) decanoic acid-treated ADSCs-EVs; (C) decenoic acid-treated ADSCs-EVs; (D) decenedioic acid-treated ADSCs-EVs; (E) sebacic acid-treated ADSCs-EVs. Data are presented as means ± SE. Statistical analysis was performed using the Tukey–Kramer test, and differences were considered significant at $p < 0.05$.

the present study have confirmed the same for the EVs (or nanoparticles) derived from any of the RJ types used in the experimental analyses here. Notably, the particle size of RJ-EVs was not different from that of ADSC-EVs, nRJ-EVs, and pRJ-EVs (Supplementary Figure 1(a)); however, significant differences in particle morphology were identified, especially in terms of cohesion. As can be observed in the TEM images (Supplementary Figure 1), several EVs present in the RJ were cohesively strung together or attached to adhesive materials derived from the hypopharyngeal or mandibular glands of the honeybee. The disintegration of this aggregate in the nRJ-EVs and pRJ-EVs was likely due to lyophilization and enzymatic treatment effects. Furthermore, the morphology of RJ-EVs was clearly different from that of ADSC-EVs, possibly because the coated EVs were primary cell-derived EVs wrapped in the RJ component (Supplementary Figure 1). Based on these morphological results, it was considered that the RJ treatment caused structural changes in ADSC-EVs, and it is reasonable to consider that the increased amount of EVs secreted by one cell increased the overall EV concentration.

The effects of EVs on NHDFs proliferation, migration ability to the wound site, and collagen production were also examined. These abilities of EVs derived from RJ-treated ADSCs were equally or significantly enhanced compared to those of conventional ADSC-EVs. The endoplasmic reticulum in cells treated with both RJ treatments was noticeably swollen compared to that of untreated cells, suggesting that the cells were in an active state of protein synthesis (Figure 2(d)); thus, the RJ treatment caused qualitative changes in ADSC-EVs. Numerous previous reports have also highlighted the roles of EVs in cell-to-cell communication, including the following: (i) EVs directly activate target cells through their cell membrane receptors; (ii) EVs transfer receptors or other proteins from donor to the target cells; and (iii) EVs can horizontally propagate

genetic information, such as DNA, mRNA, miRNA, or transcription factors to target cells [31–33]. The status of EV incorporation into NHDFs was then examined, along with the comprehensive genetic changes in cells and EVs. The membrane lipid layer of the secreted EVs was fluorescently labeled using PKH67 lipophilic dye, which stains the membrane by intercalating its aliphatic portion into the exposed lipid bilayer, and was observed using a fluorescence microscope. If EVs only transmitted signals via the ligands present on the membrane surface of the receptor cell, co-localization in the plasma membrane region could be confirmed by their binding to the membrane surface receptors; however, if EVs have been incorporated, their localization in the cytoplasm can be confirmed. As shown in the fluorescence microscopy image, after 24 h of EV treatment, all EVs were observed to be taken up by cells (Figure 2(g)). Membrane fusion and various endocytosis types (e.g., phagocytosis, macropinocytosis, and receptor- or raft-mediated endocytosis) are associated with the cellular uptake pathway, and precisely which exosomes interact with the cell depends on both the exosome and recipient cell membrane surface molecules [34, 35]. As the membrane protein profiles of the EVs and recipient cells were not analyzed in the present study, further analyses are required elucidate the mechanisms by which EVs are secreted and taken up. Regarding the changes in gene expression in ADSCs induced by the RJ treatment, the only gene that showed common variation under the same sorting conditions for both the nRJ and pRJ treatments was *SNORA2C*, a small nucleolar RNA (snoRNA). The function of SNORA2C is to chemically modify the methylation and pseudouridylation of ribosomal RNAs and other genes, which may play a major role in the splicing and processing of mature RNAs; however, this concept could not be explicitly linked to the results obtained in the present study. Getti et al. [36] reported a novel role of the *IL-33* gene (which was downregulated here and is the only protein-coding gene among the nine variable genes extracted from nRJ-treated ADSCs) where it is responsible for regulating the myofibroblast phenotype. Their study indicated that IL-33 depletion enhanced the expression of the extracellular matrix components, such as COL1A1, COL1A2, COL3A1, COL5A1, and transgelin; accordingly, it was speculated here that the reduced expression of the *IL-33* gene identified in the nRJ-treated ADSCs in the present study may be related to the increased internalization of the collagen gene cluster into the EVs. The genes related with an increased internalization in RJ-EVs included those involved in extracellular matrix synthesis (*ELN*, *SERBF1*, and *SMAD7*) [37–39], collagen metabolism (*PI16* and *CD36*) [40, 41], and cell proliferation and differentiation (*MEF2C* and *STMN2*) [42, 43], while those with a decreased internalization included those involved in collagen metabolism (*COPZ1* and *NOTCH2NLA*) [44, 45]. The GO terms in which DEGs between the nRJ- and pRJ-treated-ADSC-EVs were significantly enriched were closely associated with the extracellular matrix-related events. These results suggest that RJ enhanced the events related to the extracellular matrix of ADSCs, and in particular, the internalization of extracellular matrix- (ECM-) related genes into EVs. Based on the KEGG database, it was discovered here that the DEGs were principally enriched in the ECM-receptor interaction. Furthermore, the PI3K-Akt signaling pathway can act on certain downstream targets, including cyclin D1, glycogen synthase kinase 3β (GSK3B), and mammalian target of rapamycin (mTOR) to induce cell growth regulation and the production of various proteins. The fact that both RJ treatments enhanced the ADSC proliferation, in addition to the EVs isolated from ADSCs treated with RJ enhancing the cell proliferation and collagen production of NHDFs, is consistent with the GO and KEGG results. In particular, EVs showed an increased internalization of genes related with ECM-receptor interactions and the PI3K-Akt signaling pathway, suggesting that EVs induce ECM production as well as the cell growth (survival) system in the receptor cells.

As the miRNAs in EVs regulate the expression of genes that control various physiological phenomena in donor cells, the differences in the miRNA content in ADSCs were examined [46, 47]. Hierarchical clustering analysis revealed that both ADSCs and the secreted EVs could be classified into approximately four clusters showing relatively similar gene expression patterns. MicroRNA-205-5p is highly expressed in human epithelial tissues, such as the breast, prostate, skin, eye, and thymus tissues, and plays an important role in tissue morphogenesis as well as homeostasis. The *in silico* analysis of the miRNA-205-5p target genes using TargetScan human released *v*.8.0 (https://www.targetscan.org/vert_80/) revealed that two transcription factors repressing E-cadherin, collagen, and other polar genes, zinc finger E-box-binding homeobox 1 (ZEB1) and ZEB2, SMAD2, and SMAD4, are involved in collagen production via the transforming growth factor-β (TGF-β)/SMAD signaling pathway, whereas phosphatase and tensin homolog, a negative regulator of the phosphoinositide 3-kinase (PI3K)/AKT signaling pathway, were direct target genes [48–51]. As these genes are deeply involved in collagen production, the increased expression of miRNA-205-5p in ADSCs and its internalization into EVs induced by nRJ and pRJ treatments suggest that it may enhance skin homeostasis function through ECM production. In our study, introduction of Anti-miR-205-5p in NHDFs significantly attenuated nRJ-ADSC-EVs or pRJ-ADSC-EVs stimulated intracellular collagen synthesis. This suggests that upregulation of miRNA-205-5p caused by incorporation of EVs in NHDFs was not irrelevant to intracellular collagen synthesis. However, based on the rate at which Anti-miR-205-5p inhibits nRJ- or pRJ-ADSC-EVs induced collagen synthesis, it could be inferred that the increase in intracellular miRNA-205-5p levels caused due to EVs propagation was not the only determinant of collagen synthesis (Figure 6). The real-time PCR results also showed that miRNA205-5p was highly expressed in RJ-treated ADSCs and internalized into their EVs. This suggested that miRNA205-5p may function as a marker of EV quality capable of confirming whether EVs can enhance the function of NHDFs via RJ treatment when considering its use in future skin care product development. Furthermore, as mentioned above, miRNA205-5p is deeply involved in collagen production, suggesting that it could be

applied to nucleic acid medicine for skincare product development. In addition, miRNA-141-3p, miRNA-191-5p, and miRNA-342-3p, which maintain a decreased intracellular and EV expression, inhibit the growth and migration of fibroblasts, gastric cancer cell proliferation, and kidney fibrosis by targeting growth factor receptor binding 2-associated binding protein 1 (GAB1), cyclin-dependent kinase 6 (CDK6), and SOX6, respectively [52–54]. Notably, a decreased expression of these miRNAs involved in cell proliferation and collagen production marks an important event. These mRNAs are also expected to be used as quality control markers for the commercial use of RJ-EVs and miR-205-5p.

In conclusion, although it has previously been reported that the EVs derived from ADSCs exhibit wound-healing effects [55, 56], RJ may enhance skin homeostatic function through ECM synthesis induction by ADSCs and is anticipated to have strong applicability to the cosmetic and regenerative medicine fields; however, it remains unclear which RJ components enhance skin homeostatic function of ADSCs or induce the secretion of EVs. EV secretion was lower in the pRJ-treated ADSCs than in the nRJ-treated ADSCs, suggesting that the protein components in RJ are closely involved in EV secretion, yet as the collagen synthesis did not change between the NHDFs treated with nRJ-treated ADSC-EVs and those treated with pRJ-treated ADSC-EVs, other non-protein components may be involved in this process. To enable the use of EVs in skin care products and nucleic acid medicine, further studies are needed on various aspects, including the active components in RJ, the activation mechanism of EV secretion, and the various functional enhancement mechanisms in NHDFs induced by RJ-ADSC EV treatment.

Abbreviations

ADSCs: Adipose-derived stem cells
DEGs: Differentially expressed genes
EVs: Extracellular vesicles
NHDFs: Normal human fibroblasts
NTA: Nano tracking analysis
RJ: Royal jelly
SEM: Scanning electron microscopy
TEM: Transmission electron microscopy.

Data Availability

The data that support the findings of this study are not openly available due to sensitivity and are thus available from the corresponding author upon reasonable request.

Disclosure

The sponsor had no control over the interpretation, writing, or publication of this work.

Conflicts of Interest

Nobuaki Okumura and Tomomi Degawa are employees of Yamada Bee Company Inc. (Affiliation: Institute for Bee Products and Health Science). Tomohiro Itoh received a research grant from Yamada Bee Company Inc. Yuko Ito and Yukihiro Akao declare that there are no conflicts of interest regarding the publication of this paper.

Authors' Contributions

Tomohiro Itoh, Tomomi Degawa, and Nobuaki Okumura were responsible for study planning and design. Tomohiro Itoh, Yuko Ito, and Yukihiro Akao carried out all cellular experiments. Tomohiro Itoh and Nobuaki Okumura prepared RJ for analysis. All authors assisted in drafting and revising the manuscript.

Acknowledgments

This study was funded by Yamada Bee Company Inc.

Supplementary Materials

Supplementary Figure 1: (a) the particle distribution of FRJ EVs, nRJ EVs, and pRJ EVs measured by NTA; (b) representative SEM and TEM micrographs of prepared RJ EVs. Scale bar = 1 μm (SEM, upper panel), 200 nm (TEM, lower panel). Supplementary Figure 2: original western blot images. Original scan of the western blot is displayed in Figure 2(f). Supplementary Figure 3: fluorescence microscopic observation images of the subcellular localization of incorporated-ADSC EVs in NHDFs. Nuclei (blue): Hoechst33342, cell membrane (red): CellROX™ Deep Red, and EVs (green): PKH67. (i) ADSC EVs, (ii) nRJ-ADSC EVs, and (iii) pRJ-ADSC EVs, scale bar = 50 μm. Supplementary Table 1: list of top 20 differentially expressed genes between ADSCs EVs and royal jelly treated ADSCs EVs. Supplementary Table 2: gene ontology (GO) enrichment analysis based on 3 functional groups (biological processes (BPs), cellular components (CCs), and molecular functions (MFs)) in EVs isolated from RJ-treated ADSCs. Supplementary Table 3: Kyoto Encyclopedia of Genes and Genome (KEGG) pathway enrichment analysis of genes differentially expressed in EVs isolated from RJ-treated ADSCs. (*Supplementary Materials*)

References

[1] G. van Niel, G. D'Angelo, and G. Raposo, "Shedding light on the cell biology of extracellular vesicles," *Nature Reviews Molecular Cell Biology*, vol. 19, no. 4, pp. 213–228, 2018.

[2] L. Ginini, S. Billan, E. Fridman, and Z. Gil, "Insight into extracellular vesicle-cell communication: from cell recognition to intracellular fate," *Cells*, vol. 11, no. 9, p. 1375, 2022.

[3] L. Mazini, L. Rochette, M. Amine, and G. Malka, "Regenerative capacity of adipose derived stem cells (ADSCs), comparison with mesenchymal stem cells (MSCs)," *International Journal of Molecular Sciences*, vol. 20, no. 10, p. 2523, 2019.

[4] C. F. Chen, C. C. Hu, C. T. Wu et al., "Treatment of knee osteoarthritis with intra-articular injection of allogeneic adipose-derived stem cells (ADSCs) ELIXCYTE®: a phase I/II, randomized, active-control, single-blind, multiple-center

clinical trial," *Stem Cell Research & Therapy*, vol. 12, no. 1, p. 562, 2021.

[5] B. S. Park, K. A. Jang, J. H. Sung et al., "Adipose-derived stem cells and their secretory factors as a promising therapy for skin aging," *Dermatologic Surgery*, vol. 34, no. 10, pp. 1323–1326, 2008.

[6] X. Shen, Y. Du, W. Shen, B. Xue, and Y. Zhao, "Adipose-derived stem cells promote human dermal fibroblast function and increase senescence-associated β-galactosidase mRNA expression through paracrine effects," *Molecular Medicine Reports*, vol. 10, no. 6, pp. 3068–3072, 2014.

[7] L. Mazini, L. Rochette, and S. Amal, "Adipose derived stem cells (ADSCs) immunomodulation impact on skin tissue repair," *J Embryol Stem Cell Res*, vol. 4, no. 1, Article ID 000136, 2020.

[8] H. Zhao, Q. Shang, Z. Pan et al., "Exosomes from adipose-derived stem cells attenuate adipose inflammation and obesity through polarizing M2 macrophages and beiging in white adipose tissue," *Diabetes*, vol. 67, no. 2, pp. 235–247, 2018.

[9] H. Qiu, S. Liu, K. Wu, R. Zhao, L. Cao, and H. Wang, "Prospective application of exosomes derived from adipose-derived stem cells in skin wound healing: a review," *Journal of Cosmetic Dermatology*, vol. 19, no. 3, pp. 574–581, 2020.

[10] W. Gao, X. Wang, Y. Si et al., "Exosome derived from ADSCs attenuates ultraviolet B-mediated photoaging in human dermal fibroblasts," *Photochemistry and Photobiology*, vol. 97, no. 4, pp. 795–804, 2021.

[11] Z. Weiliang and G. Lili, "Research advances in the application of adipose-derived stem cells derived exosomes in cutaneous wound healing," *Annals of Dermatology*, vol. 33, no. 4, pp. 309–317, 2021.

[12] B. Wu, J. Feng, J. Guo et al., "ADSCs-derived exosomes ameliorate hepatic fibrosis by suppressing stellate cell activation and remodeling hepatocellular glutamine synthetase-mediated glutamine and ammonia homeostasis," *Stem Cell Research & Therapy*, vol. 13, no. 1, p. 494, 2022.

[13] J. Sanz-Ros, N. Romero-Garcia, C. Mas-Bargues et al., "Small extracellular vesicles from young adipose-derived stem cells prevent frailty, improve health span, and decrease epigenetic age in old mice," *Science Advances*, vol. 8, no. 42, Article ID eabq2226, 2022.

[14] J. W. Wang, Y. Z. Zhu, J. Y. Ouyang et al., "Adipose-derived stem cell extracellular vesicles improve wound closure and angiogenesis in diabetic mice," *Plastic and Reconstructive Surgery*, vol. 151, no. 2, pp. 331–342, 2023.

[15] N. Hu, Z. Cai, X. Jiang et al., "Hypoxia-pretreated ADSC-derived exosome-embedded hydrogels promote angiogenesis and accelerate diabetic wound healing," *Acta Biomaterialia*, vol. 157, pp. 175–186, 2023.

[16] T. Sugiyama, K. Takahashi, and H. Mori, "Royal jelly acid, 10-hydroxy-trans-2-decenoic acid, as a modulator of the innate immune responses," pp. 368–376, 2012.

[17] G. Lercker, P. Capella, L. S. Conte, F. Ruini, and G. Giordani, "Components of royal jelly II. The lipid fraction, hydrocarbons and sterols," *Journal of Apicultural Research*, vol. 21, no. 3, pp. 178–184, 1982.

[18] T. Nagai and R. Inoue, "Preparation and the functional properties of water extract and alkaline extract of royal jelly," *Food Chemistry*, vol. 84, no. 2, pp. 181–186, 2004.

[19] M. F. Ramadan and A. Al-Ghamdi, "Bioactive compounds and health-promoting properties of royal jelly: a review," *Journal of Functional Foods*, vol. 4, no. 1, pp. 39–52, 2012.

[20] S. Koya-Miyata, I. Okamoto, S. Ushio, K. Iwaki, M. Ikeda, and M. Kurimoto, "Identification of a collagen production-promoting factor from an extract of royal jelly and its possible mechanism," *Bioscience, Biotechnology, and Biochemistry*, vol. 68, no. 4, pp. 767–773, 2004.

[21] N. Hattori, H. Nomoto, H. Fukumitsu, S. Mishima, and S. Furukawa, "Royal jelly and its unique fatty acid, 10-hydroxy-trans-2-decenoic acid, promote neurogenesis by neural stem/progenitor cells *in vitro*," *Biomedical Research*, vol. 28, no. 5, pp. 261–266, 2007.

[22] V. R. Pasupuleti, L. Sammugam, N. Ramesh, and S. H. Gan, "Honey, propolis, and royal jelly: a comprehensive review of their biological actions and health benefits," *Oxidative Medicine and Cellular Longevity*, vol. 2017, Article ID 1259510, 21 pages, 2017.

[23] L. Cornara, M. Biagi, J. Xiao, and B. Burlando, "Therapeutic properties of bioactive compounds from different honeybee products," *Frontiers in Pharmacology*, vol. 8, p. 412, 2017.

[24] Y. Lin, Q. Shao, M. Zhang, C. Lu, J. Fleming, and S. Su, "Royal jelly-derived proteins enhance proliferation and migration of human epidermal keratinocytes in an *in vitro* scratch wound model," *BMC Complementary and Alternative Medicine*, vol. 19, no. 1, p. 175, 2019.

[25] N. Okumura, T. Ito, T. Degawa, M. Moriyama, and H. Moriyama, "Royal jelly protects against epidermal stress through upregulation of the NQO1 expression," *International Journal of Molecular Sciences*, vol. 22, no. 23, Article ID 12973, 2021.

[26] T. Moriyama, M. Yanagihara, E. Yano et al., "Hypoallergenicity and immunological characterization of enzyme-treated royal jelly from *Apis mellifera*," *Bioscience, Biotechnology, and Biochemistry*, vol. 77, no. 4, pp. 789–795, 2013.

[27] H. Yasmin, T. Kabashima, M. S. Rahman, T. Shibata, and M. Kai, "Amplified and selective assay of collagens by enzymatic and fluorescent reactions," *Scientific Reports*, vol. 4, no. 1, p. 4950, 2014.

[28] Y. Tsuruma, H. Maruyama, and Y. Araki, "Effect of a glycoprotein (apisin) in royal jelly on proliferation and differentiation in skin fibroblast and osteoblastic cells," *Nippon Shokuhin Kagaku Kogaku Kaishi*, vol. 58, no. 3, pp. 121–126, 2011.

[29] O. J. Ramirez, S. Alvarez, P. Contreras-Kallens, N. P. Barrera, S. Aguayo, and C. M. A. P. Schuh, "Type I collagen hydrogels as a delivery matrix for royal jelly derived extracellular vesicles," *Drug Delivery*, vol. 27, no. 1, pp. 1308–1318, 2020.

[30] C. M. A. P. Schuh, S. Aguayo, G. Zavala, and M. Khoury, "Exosome-like vesicles in *Apis mellifera* bee pollen, honey and royal jelly contribute to their antibacterial and pro-regenerative activity," *Journal of Experimental Biology*, vol. 222, no. 20, Article ID jeb208702, 2019.

[31] G. Turturici, R. Tinnirello, G. Sconzo, and F. Geraci, "Extracellular membrane vesicles as a mechanism of cell-to-cell communication: advantages and disadvantages," vol. 306, no. 7, pp. C621–C633, 2014.

[32] S. Samanta, S. Rajasingh, N. Drosos, Z. Zhou, B. Dawn, and J. Rajasingh, "Exosomes: new molecular targets of diseases," *Acta Pharmacologica Sinica*, vol. 39, no. 4, pp. 501–513, 2018.

[33] J. Makarova, A. Turchinovich, M. Shkurnikov, and A. Tonevitsky, "Extracellular miRNAs and cell-cell communication: problems and prospects," *Trends in Biochemical Sciences*, vol. 46, no. 8, pp. 640–651, 2021.

[34] L. A. Mulcahy, R. C. Pink, and D. R. F. Carter, "Routes and mechanisms of extracellular vesicle uptake," *Journal of Extracellular Vesicles*, vol. 3, no. 1, Article ID 24641, 2014.

[35] L. C. Zanetti-Domingues, S. Bonner, M. L. Martin-Fernandez, and V. Huber, "Mechanisms of action of EGFR tyrosine

kinase receptor incorporated in extracellular vesicles," *Cells*, vol. 9, no. 11, p. 2505, 2020.

[36] F. Gatti, S. Mia, C. Hammarström et al., "Nuclear IL-33 restrains the early conversion of fibroblasts to an extracellular matrix-secreting phenotype," *Scientific Reports*, vol. 11, no. 1, p. 108, 2021.

[37] S. M. Mithieux and A. S. Weiss, "Elastin," *Advances in Protein Chemistry*, vol. 70, pp. 437–461, 2005.

[38] H. Zhang and N. Ta, "Effect of isopsoralen on Smad7 in osteoblastic MC3T3-E1 cells," *Experimental and Therapeutic Medicine*, vol. 14, no. 2, pp. 1561–1567, 2017.

[39] D. Dorotea, D. Koya, and H. Ha, "Recent insights into SREBP as a direct mediator of kidney fibrosis via lipid-independent pathways," *Frontiers in Pharmacology*, vol. 11, p. 265, 2020.

[40] X. Zhao, P. Psarianos, L. S. Ghoraie et al., "Metabolic regulation of dermal fibroblasts contributes to skin extracellular matrix homeostasis and fibrosis," *Nat Metab*, vol. 1, no. 1, pp. 147–157, 2019.

[41] P. Singhmar, R. T. P. Trinh, J. Ma et al., "The fibroblast-derived protein PI16 controls neuropathic pain," *Proceedings of the National Academy of Sciences of the United States of America*, vol. 117, no. 10, pp. 5463–5471, 2020.

[42] C. Chiellini, G. Grenningloh, O. Cochet et al., "Stathmin-like 2, a developmentally-associated neuronal marker, is expressed and modulated during osteogenesis of human mesenchymal stem cells," *Biochemical and Biophysical Research Communications*, vol. 374, no. 1, pp. 64–68, 2008.

[43] M. Ieda, J. D. Fu, P. Delgado-Olguin et al., "Direct Reprogramming of fibroblasts into functional cardiomyocytes by defined factors," *Cell*, vol. 142, no. 3, pp. 375–386, 2010.

[44] C. Dees, M. Tomcik, P. Zerr et al., "Notch signalling regulates fibroblast activation and collagen release in systemic sclerosis," *Annals of the Rheumatic Diseases*, vol. 70, no. 7, pp. 1304–1310, 2011.

[45] K. Kawaguchi, A. Endo, T. Fukushima, Y. Madoka, T. Tanaka, and M. Komada, "Ubiquitin-specific protease 8 deubiquitinates Sec31A and decreases large COPII carriers and collagen IV secretion," *Biochemical and Biophysical Research Communications*, vol. 499, no. 3, pp. 635–641, 2018.

[46] K. Saliminejad, H. R. Khorram Khorshid, S. Soleymani Fard, and S. H. Ghaffari, "An overview of microRNAs: biology, functions, therapeutics, and analysis methods," *Journal of Cellular Physiology*, vol. 234, no. 5, pp. 5451–5465, 2019.

[47] Q. Yao, Y. Chen, and X. Zhou, "The roles of microRNAs in epigenetic regulation," *Current Opinion in Chemical Biology*, vol. 51, pp. 11–17, 2019.

[48] K. Tsuchida, Y. Zhu, S. Siva, S. R. Dunn, and K. Sharma, "Role of Smad4 on TGF-β–induced extracellular matrix stimulation in mesangial cells," *Kidney International*, vol. 63, no. 6, pp. 2000–2009, 2003.

[49] S. K. Parapuram, X. Shi-Wen, C. Elliott et al., "Loss of PTEN expression by dermal fibroblasts causes skin fibrosis," *Journal of Investigative Dermatology*, vol. 131, no. 10, pp. 1996–2003, 2011.

[50] J. Qi, Y. Liu, K. Hu, Y. Zhang, Y. Wu, and X. Zhang, "MicroRNA-205-5p regulates extracellular matrix production in hyperplastic scars by targeting Smad2," *Experimental and Therapeutic Medicine*, vol. 17, no. 3, pp. 2284–2290, 2019.

[51] E. Ferrari and P. Gandellini, "Unveiling the ups and downs of miR-205 in physiology and cancer: transcriptional and post-transcriptional mechanisms," *Cell Death & Disease*, vol. 11, no. 11, p. 980, 2020.

[52] J. Feng, S. Xue, Q. Pang, Z. Rang, and F. Cui, "miR-141-3p inhibits fibroblast proliferation and migration by targeting GAB1 in keloids," *Biochemical and Biophysical Research Communications*, vol. 490, no. 2, pp. 302–308, 2017.

[53] N. J. Cao, H. H. Hou, and F. Li, "MicroRNA-191-5p represses cell growth by targeting CDK6 in gastric cancer," *Zhonghua Yi Xue Zhi*, vol. 100, no. 46, pp. 3689–3693, 2020.

[54] Z. H. Jiang, Y. Z. Tang, H. N. Song, M. Yang, B. Li, and C. L. Ni, "miRNA-342 suppresses renal interstitial fibrosis in diabetic nephropathy by targeting SOX6," *International Journal of Molecular Medicine*, vol. 45, no. 1, pp. 45–52, 2020.

[55] L. Hu, J. Wang, X. Zhou et al., "Exosomes derived from human adipose mensenchymal stem cells accelerates cutaneous wound healing via optimizing the characteristics of fibroblasts," *Scientific Reports*, vol. 6, no. 1, Article ID 32993, 2016.

[56] L. Wang, L. Hu, X. Zhou et al., "Exosomes secreted by human adipose mesenchymal stem cells promote scarless cutaneous repair by regulating extracellular matrix remodelling," *Scientific Reports*, vol. 7, no. 1, Article ID 13321, 2017.